



***Facultad
de
Ciencias***

**Simulación de tasas de dosis en técnicas de
braquiterapia**
(Dose rate calculations in brachytherapy)

Trabajo de Fin de Grado
para acceder al

GRADO EN FÍSICA

Autor: Rosalía Feal Calvo

Director: Ángel Mañanes Pérez

Co-Director: Jérica Sánchez Mazón

Julio – 2016

Acknowledgments

First of all I would like to express my gratitude to my two co-directors Ángel Mañanes Pérez y Jérica Sánchez Mazón for all the patience they have had with me and all their help and support both in this project and in the last subject of my degree.

Second I want to thank my family and friends for putting up with my stress and bad mood and listening to me, even if they did not understand a word I said. In particular I am deeply grateful to my friend Maria and my parents, because they listened to every single one of my rants, and there had been a few.

Resumen

Se trata de calcular, simulando la propagación y absorción de fotones gamma y de Rayos X, la dosis recibida por diferentes órganos sensibles cuando se realizan procesos de braquiterapia en el tratamiento de carcinomas de próstata usando principalmente una fuente de ^{192}Ir . En la primera parte del trabajo se revisará la técnica y se describirán los diferentes métodos de control de la dosis en órganos sensibles (organs at risk, OAR). En la segunda parte, se caracterizará, mediante simulaciones, la eficacia de diversas técnicas de protección de dichos órganos, principalmente el efecto de la inclusión de una capa de ácido hialurónico (HA) entre los órganos a tratar y los diferentes órganos sensibles.

Palabras claves: simulación, braquiterapia, OAR, protección, capa HA

Abstract

The aim of the present project is to calculate the dose rate at different organs at risk (OARs) in a brachytherapy treatment of the prostatic cancer. We shall focus on those treatments using gamma and X ray photons produced by a ^{192}Ir source. The first part of the project is the analysis of the actual techniques used to control the dose rate absorbed by the OARs. In the second part we will characterize characterize by the simulation of the propagation and absorption of gamma rays the protection effects of different methods, mainly the inclusion of a thin hyaluronic acid (HA) shell between the treated organ and the OARs.

Key words: simulation, brachytherapy, OAR, protection, HA layer

Contents

1	Introduction	3
2	Treatment plan	7
2.1	How to plan a radiation treatment for an individual patient . . .	7
2.2	How is radiation therapy given to patients	8
2.2.1	External - beam radiation therapy	9
2.2.2	Systemic radiation therapy	9
2.2.3	Internal radiation therapy	9
2.3	Technical problems in dose measurement	11
3	Prostate cancer	13
4	Dosimeters: MOSFET devices	15
4.1	General properties of dosimeters	15
4.2	MOSFET devices as dosimeters	16
4.3	Clinical application of MOSFET in HDB	19
5	Radiation theory	21
5.1	Attenuation produced by a Hyaluronic Acid layer	24
6	Simulations	27
6.1	Geometrical parameters	27
6.2	Dose at OARs without HA protection	29
6.3	Effect of the HA layer	33
7	Conclusions	36

1 Introduction

Radiation therapy or radiotherapy is a technique based on the use of ionizing radiation (high – energy radiation), and it has been a part of cancer treatments for a long time. The final aim of this procedure is to deposit a high dose of radiation, which is defined as the energy per unit mass and it is measured in Gray ($1 \text{ Gy}=1 \text{ J kg}^{-1}$), in a concentrated space (tumor), reducing to the minimum the number of viable residual cells on it, while it delivers the minimum dose possible to the healthy radiated tissue, specially, to the organs at risk (OAR) [1]. Radiation therapy kills cancer cells by damaging their DNA, which are those the molecules inside the cells that carry the genetic information and can pass it on from one generation to the next. Ionizing radiation can damage DNA directly (direct action) or it can create charged particles called free radicals within the cells, and will be turned into damage to the DNA (indirect action), as can be seen in Figure 1. When a cell’s DNA is damaged beyond repair it stops dividing, dies and it is eliminated by the body’s natural processes.

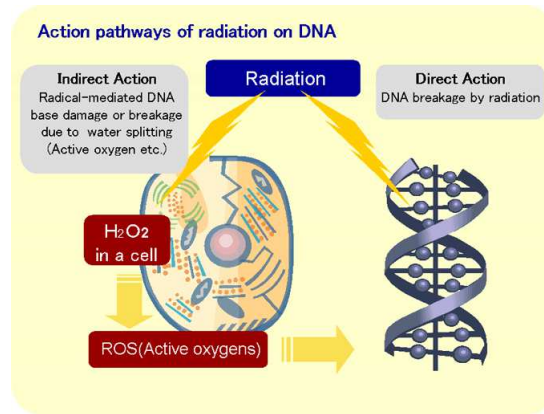


Figure 1: This figure shows the two processes of damaging a cancer cell that can occur when the cell is targeted by radiation, it can be a direct or indirect action [2].

However, not only cancer cells are being damaged, radiation therapy can also harm healthy cells, which will lead to side effects, such as loss of hair, change in skin color, impotence or infertility [3], [4]. To be able to achieve its goal the therapy has to be carefully studied and planned, which constitutes one of the most important phases of the therapy “planning and simulation”. One way to achieve delivering the minimum dose to the OAR is dividing the total dose in several sessions over time; this will favour the biological mechanisms of cell regeneration making it less likely that the healthy tissue is damaged and receives a higher dose than the one planned [1].

There are several types of radiotherapy, but the most important ones are: brachytherapy, or internal radiation therapy; and teletherapy, or external beam radiation therapy.

The first one uses a radioactive encapsulated source that is put in contact with or next to the area required to treat. In this method the irradiation only affects a localized area, since the source is placed next to the tumor, and this causes a reduction on the exposure for radiation on healthy tissues around the cancerous tumor. One of the advantages of this method is that the dose rate used can be very high, given that it is only affecting a very small area, while the probability of damage on the healthy tissues is reduced drastically. Another advantage of this method is that, even if it is distributed in time, the length in time of the treatment is shorter than other techniques, which can help reduced the chance of surviving cells dividing and growing between sessions. This type of radiotherapy is commonly used to treat cervical, prostate, breast and skin cancer.

The second type, teletherapy, uses external beams of ionizing radiation to fight the cancerous tumor from afar. The external source of radiation is pointed at the part of the body of the patient, who lays on a stretcher or sits on a couch, that needs to be treated and it directs the radiation to the tumor from outside the body. It can be superficial or deep, depending on the energy of the radiation used. The beam can be of X-ray, electrons, gamma or hadrons. This type of radiotherapy is commonly used to treat breast, lung, colon and prostate cancer [5], [6].

When a medical team is faced with a case there are several reasons to chose ionizing radiation as the best treatment for the patient, either with curative intent or with a palliative one. When it is used with curative intent is with the goal of eliminating the tumor and preventing its recurrence, therefore healing the cancer. In these cases radiation therapy can be used alone or can be combined with surgery, chemotherapy, or both. When radiotherapy is used with a palliative intent it doesn't have the intention to heal, it is simply used to alleviate symptoms and mitigate the pain and suffering occasioned by the cancer. It is commonly used to shrink tumors caused by cancer cells that had spread to the brain from another part of the body (metastases); to shrink a tumor that is pressing on the spine or growing within a bone and causing pain; or to shrink tumors near the esophagus, given that they interfere with the patient's ability to drink and eat [3].

The use of these kind of therapies require a high level of quality assurance and security. Every center that uses ionizing radiation must have a quality and control assurance program. This quality assurance program is developed as much for patients (cancer treatments and radiography patients) as for medical personal and it is highly regulated through legislation, in Spain the current law is R.D. 1132/1990 [7] and R.D. 783/2001 [8]. According to American Association of Medical Physics in Medicine (AAMP) [5] errors in treatments and receiving a higher dose that the one planned is caused by:

- Errors localizing the tumor
- Human error in equipment calibration
- Errors in the calculation of doses

- Errors in field placement

The quick implementation of new and advanced radiotherapy techniques has made the concern about quality assurance grow, in particular in the protocols. In 1976 the International Commission on Radiation Units and Measurement (ICRU) recommended an accuracy of $\pm 5\%$ in the delivery of absorbed dose. Considering all the uncertainties and errors that can be produced this level of accuracy is not easy to achieve [5].

There are several methods that allow to directly measure the dose delivered to the patient, one of them is the in vivo dosimetry. This method also allows to be aware of the precision of the treatment and the systematic errors that can occur, which will affect to the quality assurance controls done to the equipment. If the systematic errors are spotted, they can be corrected and the quality assurance of the equipment will be improved. One of the most used dosimeters in this type of dosimetry are the MOSFETs.

To be able to study and understand radiation some radiologic magnitudes and units need to be comprehended. Some of them are explained now:

- Activity A : is the number of spontaneous nuclear desintegrations per unit time that occur in a sample containing a certain amount of a radinuclide. Its unit is the Bequerel ($1 \text{ Bq} = 1 \text{ s}^{-1}$).
- Exposition X : is the amount of electric charge freed because of the action of X o γ photons in a mass of air. Its unit is the Roentgen ($1 \text{ R} = 2.58 \cdot 10^{-4} \text{ C kg}^{-1}$).
- Exposition rate \dot{X} : is the exposition produced in a certain point per unit time. It is given in R/s.
- Kerma K : is the sum of all initial kinetic energies of all of the charged particles that have been freed by uncharged ionizing particles in a material per unit mass. It is measured in rad or Gray ($1 \text{ Gy} = 1 \text{ J kg}^{-1}$). The equivalence between them is given by $1 \text{ Gy} = 100 \text{ rad}$.
- Absorbed dose \dot{D} : is the mean energy transferred by any ionizing radiation to a material per unit mass. It is also measured in Gy.
- Absorbed dose rate D : is the absorbed dose in a time interval. Its unit is Gy/s.
- Equivalent dose H : is the absorbed dose measured in biological tissue. It is used to evaluate the biological effects induced by the absorbed radiation. The relation between D and H is given by a weighting factor W_R , that changes depending on the type of radiation and the energy, as can be seen in Figure 2 . Its unit is the Sievert (Sv). When the radiation used is γ photon then $1 \text{ Sv} \simeq 1 \text{ Gy}$.

In cancer treatments radiation doses are measured in gray, which constitutes the amount of radiation energy absorbed in 1 kg of human tissue. To kill different type of cancer cells different doses of radiation are needed.

Type of radiation, R	Energy range	Quality or weighting factor, w_R
Photons, electrons	All energies	1
Neutrons	<10 keV	5
	10–100 keV	10
	100 keV–2 MeV	20
	2–20 MeV	10
	>20 MeV	5
Protons	<20 MeV	5
Alpha particles, fission fragments, heavy nuclei		20

Figure 2: This figure shows the values of the radiation weighting factor depending on the type of radiation (photons, neutrons, alpha particles) and depending on the energy used [9].

The main goal of this work is to study the OARs' absorbed dose in a brachytherapy treatment for prostate cancer. As it has been stated before quality assurance is very important in a cancer treatment, and that $\pm 5\%$ accuracy in the dose delivered to the tumor recommended by the ICRU needs to be controlled. But in this project the goal was not to study the absorbed dose of the treated tumor, it was to study the absorbed dose in the OARs, so the dose delivered to the OARs has to be controlled as well. In general, when programming a treatment, the protection of the OARs is established following the ALARA principle, which means "As Low As Reasonably Achievable", but recently there have been more and more studies about the dose limitation in OARs. One of the purposes of this project is to evaluate in a realistic way the actual dose at the OARs and also to calculate the protection effects through a comparison of the absorbed dose when there is no protection between the prostate and the walls of the rectum in the form of a layer of hyaluronic acid, and the absorbed dose when there is protection. In addition, a simulation of how does the absorbed dose change in these two cases with different irradiation sources is made. The study of the different cases will be made through a MatLab program.

For realistic radiotherapy treatments [10], it has been established that the dose limitation for the rectum is 70 Gy for 10 – 15% of the volume, taking into account that there cannot be more than 50 Gy for 50% of the volume. It is also stated that the penis bulb, which includes the urethra, cannot surpass 50 Gy for 95% of its volume. These values give the reference to check our simulations because they are a maximum that cannot be exceeded in any actual treatment.

2 Treatment plan

2.1 How to plan a radiation treatment for an individual patient

When a patient is diagnosed cancer its physician alongside with the medical physicist develop the best treatment plan to be able to get rid of the cancerous cells at the same time that the healthy ones suffer the minimal damage. This phase is called 'treatment planning', and begins with simulation, which is the process used to plan the therapy and to make sure the target is precisely located and marked. This is the phase where detailed image scans of the patients are made, which are used to know for certain where is the tumor located, what is its size and what organs at risk (OAR) are around. These images are usually obtained through computed tomography (CT) scans, which get pictures of the inside of the body by an X – ray machine connected to a computer. There are others techniques that can be used, like magnetic resonance imaging (MRI), positron emission tomography (PET) or ultrasound scans [3].

Simulation is one of the most important parts of the treatment, given that with it the medical physicist is able to know where is placed the tumor and its dimensions; because of its importance it is necessary that the results obtained are as close to reality as possible. To be able to obtain good results it is crucial that the patient stays in the same position for as long as the imaging lasts, either face up, face down or sideways, depending on where is the tumor located. The position must be held for 15 to 30 minutes, so it has to be comfortable, but it has to optimize the treatment too [11]. This usually means that the patient has to be immobilized with a special cushion – like device or body mold that holds its shape, as can be seen in Figure 3 (a). If the radiation is being directed to the head or neck the patient will need to wear a thermoplastic mask, which will be molded to the face, or even shoulders, and secured to the table, as shown in Figure 3 (b).



Figure 3: This figure shows the cushion – like mold used to keep the patient in the same position for the duration of the simulation and every session of the treatment (a); and the thermoplastic mask molded to the patient's face (b) [12].

When the patient is correctly positioned the radiation therapy team uses a combination of laser lights and markers on the patient's body to indicate the area of study and to help align the patient's body, then they will take CT images of this area. Once the image is obtained the medical physicist can determine the exact area of the tumor, therefore the exact area that will need to be treated. Then a treatment plan will be composed by the physician and the medical physicist, this plan will determine the total dose radiation that will be delivered, the

number of beams that will be used, in which angles they will be delivered, how many sessions will be needed, how much dose will be delivered to the OARs and what protections will be necessary. This plan needs to be approved by the physician, if it isn't then it must be redone following the physician's instructions. If the plan is approved then the treatment can start, with the appropriate verifications of the absorbed dose. During the treatment the patient will be placed on a table in the same position of the simulation, with the same restraining devices.

As it has been stated before, there are some healthy organs that receive radiation which have to be protected, these organs are labeled as organs at risk (OAR). On top of that there are some organs that are more sensible to radiation and more prone to be damaged, for example reproductive organs. This has to be taken into account in the planning of the treatment and the protection. In addition, if the patient has already been treated with radiation that area may not be possible to treat again, and an alternative treatment will have to be found. When the area to be treated is selected it usually includes the tumor and a halo of healthy tissue to keep in mind the movements of the body when the patient is breathing and the movements of the organs within the body, which are completely normal and can change the placement of the tumor in between the sessions. Another reason why this halo is included in the treatment is to reduce the chance of tumor recurrence from cancer cells that have spread to the normal tissue next to the tumor (microscopic local spread).

2.2 How is radiation therapy given to patients

The most common types of radiation therapy are: external – beam radiation, in which the radiation comes from a machine outside the body; and brachytherapy or internal radiation therapy, in which the radiation comes from the radioactive material placed in the body near the tumor or cancer cells. Another important type is systematic therapy which uses radioactive substances that travel through the bloodstream reaching and attacking cells throughout the body [3].

There are several factors that make physicians and medical physicist choose what type of therapy should be used, some of these factors are:

- The type of cancer
- The size and location in the body of the cancer
- How close is to normal or healthy tissues sensitive to radiation
- How far in the body the radiation needs to travel
- The patient's general health and medical history
- Whether or not the patient will have other types of cancer treatments

2.2.1 External - beam radiation therapy

It is one of the most common and used type of radiation therapy to fight cancer, it uses a machine placed outside the body to send radiation toward the cancer, which it is usually delivered in the form of photon beams, it can be either X – rays or gamma rays.

Many types of external – beam radiation therapy are delivered using a machine called linear accelerator (LINAC), which uses electricity to create a stream of fast – moving subatomic particles creating a high – energy radiation used to treat cancer. This radiation treatment is highly studied and it usually is given in daily treatment sessions over the course of several weeks. The number of sessions depend on many factors, including the total radiation dose that will be given, the location, size and stage of the tumor [3].

Its main advantage is that the radiation beams are shaped to fit the tumor. Because of this, there are several kinds of radiation methods, like:

- 3D – CRT: Three dimensional conformal radiation therapy
- IMRT: Intensity – modulated radiation therapy, which uses hundreds of tiny collimators to deliver a single dose of radiation. It reduces the risks of side effects.
- IGRT: Image - guided radiation therapy, during the treatment repeated imaging scans are performed; these are processed by computers to identify changes in tumor’s size and location due to treatment. This will allow to change the position or adjust the planned radiation dose of the treatment.
- Tomotherapy: is a type of image – guided IMRT. This machine is a hybrid between a CT imaging scanner and an external – beam radiation therapy machine. The machine can rotate and captures CT images of the patient’s tumor immediately before the treatment sessions to allow very precise targeting of tumor and spare the healthy tissue.
- SRS: Stereotactic radiosurgery can deliver one or more high doses of radiation to a small tumor. It uses extremely accurate image – guided tumor targeting and patient positioning. Therefore, a high dose of radiation can be given without excess damage to normal tissue.

2.2.2 Systemic radiation therapy

In this type of therapy the patient swallows or is injected the radioactive substance. It is habitually used in thyroid cancer, with Iodine (^{131}I), given that this gland adsorbs this isotope naturally.

2.2.3 Internal radiation therapy

Also known as brachytherapy, from the greek “brachios”, which means short, is a technique that consists in delivering radiation using sources (radioactive materials) placed next to the tumor, which means that the source is inside

the patient. There are several brachytherapy techniques, such as interstitial brachytherapy, in which the source is placed within tumor tissue, like prostate; intracavitary brachytherapy, in which the source is placed within a surgical or body cavity, like chest cavity; and episcleral brachytherapy, which is used to treat melanoma inside the eye.

In brachytherapy the radioactive sources are called “seeds”, and are placed inside the patient using needles, catheters or other kind of delivering device. A radioactive isotope decays naturally and in this process it emits radiation that will damage the DNA of the cancer cells. The seeds can stay inside the patient’s body a long time, because after it decays completely it won’t emit radiation, and it won’t represent a danger.

It has been proved that brachytherapy can deliver higher doses of radiation and cause less damage to the healthy tissue than external-beam radiation therapy for the same cancer. There are several ways to classify brachytherapy [3], one of the is due to dose rate:

- Low – dose – rate: in this treatment cancer cells receive a continuous low – dose radiation from the source over a period of several days. Dose rates 0.4 – 2 Gy/h.
- Medium – dose – rate: in this treatment cancer cells receive radiation that can be delivered by manual or automatic afterloading, although the latter is far more frequent. Dose rates 2 – 12 Gy/h.
- High – dose – rate (HDB): in this treatment a robot machine places and removes the source from within the patient in each session. This kind of treatment usually entails several sessions. Dose rates > 12 Gy/h.

Another way of classifying brachytherapy is due to placement of the source:

- Temporary: this technique uses a delivering device and carrier, such as catheters, to place the source and to remove it in each session. It can be used both in low – dose and high – dose – rate brachytherapy.
- Permanent: in this technique the sources are surgically sealed within the body and left there. This one only can be used in low – dose – rate brachytherapy.

Brachytherapy can be used alone or combined with surgery, chemotherapy, or external – beam radiation therapy. In early – stage prostate cancer, the radioactive sources are needles inserted through the skin between the scrotum and the rectum. The placement of these needles is done with the help of transrectal ultrasound or computed tomography to be able to have an image of the body’s interior. This is the case that will be studied in the simulation.

In this work a simulation of brachytherapy treatment of prostate cancer is studied; for this kind of cancer the type of brachytherapy used is high – dose –

rate with temporary placement of the source, since is one of the most technologically advanced brachytherapy method [13]. In high – dose – rate brachytherapy a unit contains a small, but very active ^{192}Ir source, that can be placed in the desired anatomy with pinpoint accuracy for each prescribed dwell or residence position using a computer. Distribution of absorbed dose is determined with the dwell positions and the time in which the source is in every position, obtained from a real treatment. This process will be detailed when the simulation is explained in section 6.

The basic principle of curative radiation is to deliver the maximum dose to cancer cells, also called target tissue; but maintain the healthy tissues free of radiation to the extent possible, therefore, obtain the best therapeutic ratio. The main advantages of high – dose brachytherapy [5] are:

1. A great amount of dose can be delivered to a reduced zone, given that the source is in contact with the tumor.
2. Dose distribution can be modified changing either dwell positions or dwell time; this optimizes dose distribution in the tumor volume.
3. It is a short treatment when compared with external – beam radiation, leading to a reduction of expenses and it can applied to more patients.

2.3 Technical problems in dose measurement

Dose measurement in high – dose brachytherapy with a ^{192}Ir source can be quite difficult due to several factors:

- Energy dependence: the energy spectrum of ^{192}Ir is complicated, as can be seen in Figure 4. It has about 24 photon decays with energies between 9 and 100 keV. However, there are two decays that disappear once the source is encapsulated, and because of this the air kerma of the source weighted average energy is about 397 keV. In this energy range dosimeters present a clear energy dependence.
- High dose gradient near the source: absorbed dose in tissues varies as a function of the distance to the source (inverse square law). In brachytherapy the distance varies between 1 and 5 cm, this is because of the high gradient near the source that leads to errors in dose measurement, and is complicated to get a proper accuracy.

In vivo dosimetry is the most indicated one to verify the absorbed dose in patients. *In vivo* dosimetry refers to measuring the dose received by the patient during treatment. This is different to *in vitro* dosimetry, which refers to most other physics measurements in phantoms. Doses at depth are difficult, if not impossible, to obtain without invasive procedures [14].

Most of the treatments are planned in several sessions, and even though this may be a nuisance for the patient is done this way for two determining reasons, to minimize the damage caused to the normal and healthy tissue, and

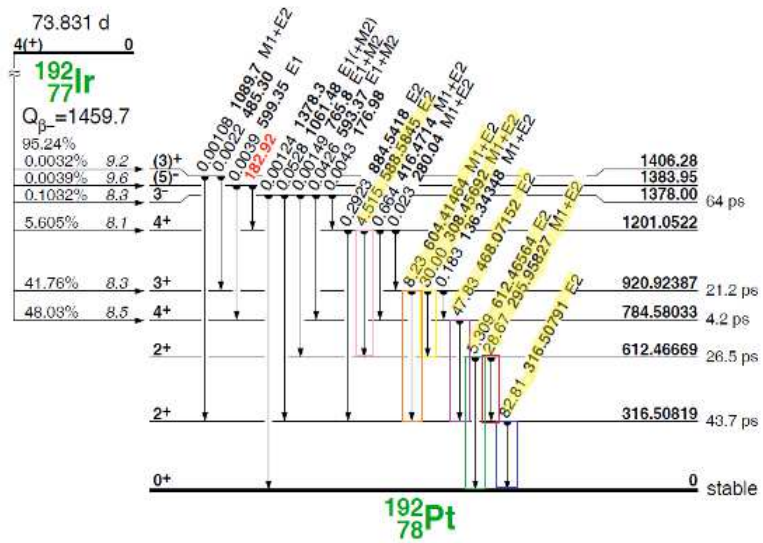


Figure 4: This figure shows the complete energy spectrum of ^{192}Ir with its most intense gamma rays marked in different colours.

to increase the probability of cancer cell exposition to radiation in the point of the cell cycle in which is most likely to have its DNA damaged.

3 Prostate cancer

Prostate cancer is a condition in which malignant cells form in the tissues of the prostate. The prostate is a gland that is part of the male reproductive system, its diameter is around 5 cm, it is placed just below the bladder and in front of the rectum. The anatomy of the male reproductive system can be seen in Figure 5. The dose rate that arrives to these two organs will have to be carefully monitored during the cancer treatment, given that bladder, rectum and urethra will be the organs at risk (OAR). It is one of the most common cancers in older men. Some of the symptoms are weak flow of urine, frequent urination, blood in the urine or semen and pain while urinating. Apart from cancer, other conditions may cause these symptoms, given that as men grow older the prostate can get bigger and it can block the urethra or bladder, as can be seen in Figure 6. This condition is called “Benign prostatic hyperplasia (BPH)”, and it needs surgery to be fixed [15].

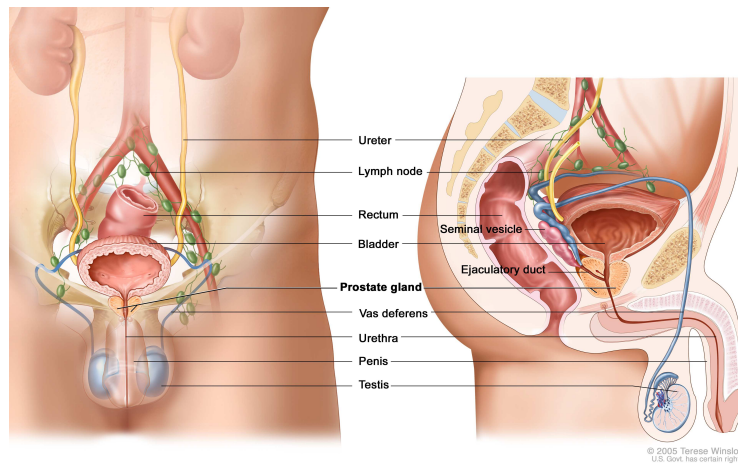


Figure 5: This figure shows the anatomy of the male reproductive system in two perspectives; at the left is the front perspective and at the right is the side perspective. These two perspectives give a better understanding of the geometry that has to be simulated [15].

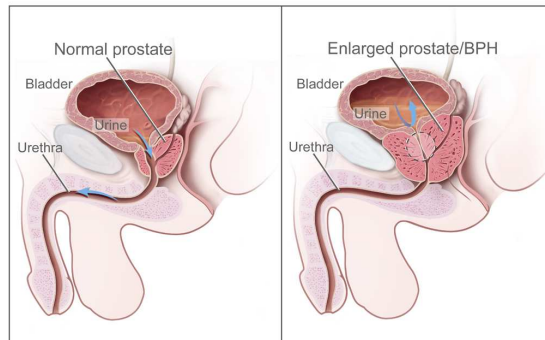


Figure 6: This figure shows a normal prostate (left) and a prostate affected by BPH (right).

There are different kind of treatments for patients with prostate cancer, some are standard and some are being tested in clinical trials. The most used standard treatments [15] are watchful waiting or active surveillance, surgery, hormone therapy, chemotherapy and radiation therapy. The focus will be on the last one, this type of cancer treatment uses high – energy X – rays and other kind of radiation to kill cancer cells or to keep them from growing. As it has been stated before, there are two forms of radiation therapy, external – beam radiation therapy and brachytherapy, which is the one that will be used in the simulation made for this work. This type of treatment can provoke urinary problems and it increases the risk of having bladder or gastrointestinal cancer.

4 Dosimeters: MOSFET devices

4.1 General properties of dosimeters

An ideal dosimeter is one that is sensible to radiation and is able to measure, directly or indirectly, dosimetric quantities, such as exposition (this magnitude represents the quantity of electric charge liberated because of the action of X or γ photons in a mass of air) and absorbed dose (this magnitude represents the mean energy transferred by any ionizing radiation to matter per mass unit) [1]. It also must fulfill a series of characteristics [5]:

1. Accuracy and precision: in radiation therapy the uncertainty associated to measurements is expressed in terms of accuracy and precision. Accuracy describes how close is the expected value of the quantity measured to the real value, while precision is the ability to reproduce the measurements under similar conditions. Ideally a dosimeter should be accurate and precise.
2. Linearity: the reading of the dosimeter should be linearly proportional to the quantity measured, but beyond a certain range of dose it has a non-linear behavior, that usually can be fixed.
3. Dose rate dependence: an ideal dosimeter should be independent of the dose rate, meaning that its response should be the same for two different dose rates. However, the truth is that dose rate can affect dosimeter's reading.
4. Energy dependence: ideally, the energy dependence should be non – existent, however, dosimeters usually are calibrated to an specific radiation beam (for example, ^{60}Co) and then are used in a energy range higher than the one they were calibrated for.
5. Directional dependence: it is the variation of a dosimeter's response as the radiation's incident angle varies. Ideally a dosimeter should have an isotropic response in 360° , but sometimes it can have a directional dependence because of the construction, the size or the energy of the incident radiation.
6. Spatial resolution and physical size: a dosimeter should have a dose read-out in a small volume, in essence, a point dose. This is important, specially to be able to make measurements in a rapid dose fall – off region. The problem is that the construction of a “point dosimeter” is highly complicated, given that small size goes hand in hand with a high signal – noise ratio.

Obviously all dosimeters cannot fulfill all these characteristics, what it is usually done is choose the ones that are important for a certain treatment and improve them.

4.2 MOSFET devices as dosimeters

In this section we describe the general properties of MOSFET devices for its use as dosimeters. In spite of the fact that we have not performed actual measurements of the dose at OARs, these devices are the state of the art to obtain that kind of information to be checked with the results of our simulations.

The latest technological developments in dosimetry techniques have allowed the introduction of MOSFET detectors. A MOSFET is a metal oxide semiconductor field effect transistor used for amplifying or switching electronic signals, its basic principle is the change of the threshold voltage (V_{th}) induced by ionizing radiation. When used as dosimeter MOSFET can operate in passive or active mode, the first one is without bias voltage on the gate and the second one is with a positive or negative gate bias voltage. The change in the threshold voltage results as proportional to the absorbed dose and the change must be measured when the intensity that goes through the detector is constant, as can be seen in Figure 7. When the MOSFET is operating in active mode the threshold voltage is a linear function of the absorbed dose. The main advantages of MOSFET detectors are their really small size (microMOSFET 3.5 mm), that it gives an immediate lecture of the measurements and their capacity of measuring dose immediately after or even during irradiation. These advantages make MOSFETs a useful tool for *in vivo* and on – line dosimetry [5], [16], [17].

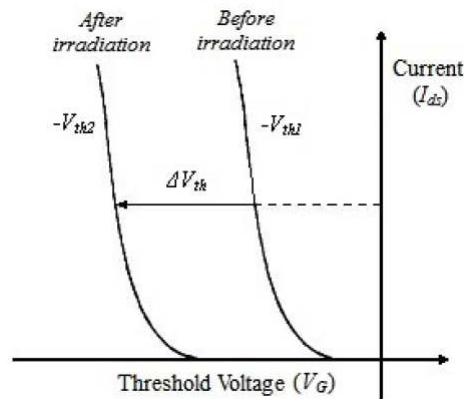


Figure 7: This figure shows the relation between the current going through the MOSFET (Y – axis) and the threshold voltage (X – axis) [5]. The variation of the threshold voltage before being irradiated V_{th1} and after being irradiated V_{th2} is what is proportional to the absorbed dose.

The MOSFET detector was first created by Dr. Andrew Holmes-Sielde in 1978, and its use as dosimeter was a byproduct of the analysis of the effects that radiation produces in equipments placed in outer space. With time their uses have increased, now they are used in microprocessors and radio-frequency amplifiers, for example. A MOSFET is a four – terminal device composed of:

- a source (S)

- a drain (D)
- a metal gate (G)
- a semiconductor substrate (SB)

The part of the semiconductor immediately under the metallic gate connects the source and the drain and it's called *channel region*. All parts of the MOS-FET and their setting can be seen in Figure 8.

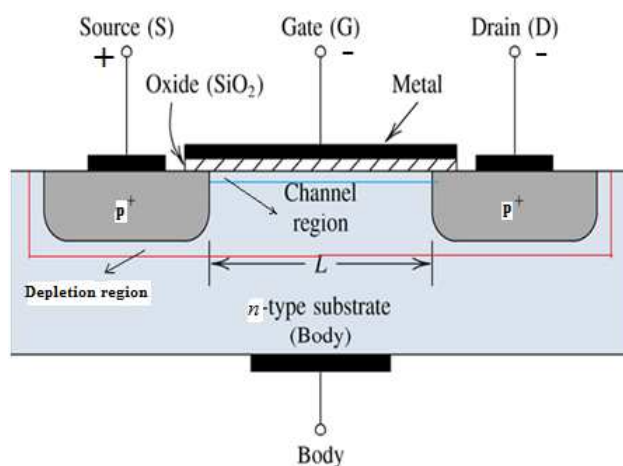


Figure 8: This figure shows a P – channel MOSFET detector in which all parts are visible and labeled [5].

Depending on the kind of charge carriers conducted in the channel region MOSFETs [5] are classified in:

- P-channel: this type of MOSFET can be seen in Figure 8. This type of MOSFET is based on hole's conduction, is built on a substrate of silicon doped with donor impurities (n- type), on top of which there are two regions of highly doped acceptor impurities (p+ type); the source and the drain metallic contacts are placed on top of the p type regions, and the gate contact is between them. The gate is separated from the n type substrate by an insulating silicon dioxide layer. "When the gate voltage (V_G) is set to zero, the source – drain current is limited by only a minimal amount of reverse saturation current from the two back – to – back p – n junctions. The device is therefore in its "off" state." [5] If a small and negative voltage is applied to the gate a large amount of the majority carriers in the channel under the gate oxide (electrons) will be depleted. This is caused by the electric field from the negative gate charge. This *depletion region* acts as an insulator, so the source – drain current generated is negligible. If the negative voltage applied is sufficiently high a great amount of the minority carriers (holes) are attracted to the oxide – silicon interface from the silicon substrate, the drain and the source regions. Once the concentration of

holes is sufficiently high a conduction channel will be formed, causing the apparition of an appreciable source – drain current (I_{ds}). In this case the device is in its “on” state. Therefore, the minimum voltage V_G needed to start an appreciable current will be the threshold voltage of the device (V_{th}).

- N – channel: electron’s conduction, it’s similar to the p – channel MOSFET, but the voltage polarity and the sign of the charge carriers is opposite.

MOSFET dosimetry is based on the generation of pairs electron – hole in the silicon dioxide (SiO_2), caused by the ionizing radiation reaching it. The energy needed to generate a pair of electron – hole is $E \simeq 18$ eV, as explained in [18]. When the radiation arrives to the MOSFET detector the negative charges are knocked out of the atoms in the SiO_2 layer, causing the apparition of positively charged holes. “The generated electrons, whose mobility in SiO_2 at room temperature is about 4 orders of magnitude greater than holes, quickly move toward the gate electrode. The holes that escape initial recombination, on the other hand, are relatively immobile and remain behind, near the point of generation.” [19]. At room temperature and when the period is $T \simeq 1s$ the holes suffer an stochastic hopping in the direction of the interface Si – SiO_2 , where they are restrained in long – term trapping sites within the oxide. This will cause a buildup in the positive charge Q_T . This residual positive charge will change the current in the channel, and to be able to guarantee that there is a constant current flow in the channel is necessary a corresponding negative shift in the threshold voltage at the gate (ΔV_{th}). This negative shift in the threshold voltage is proportional to the total number of trapped charges, which is proportional to the radiation dose deposited in the oxide layer.

When the electron – hole pairs have been generated within the SiO_2 layer, a small fraction of these electrons and holes will recombine depending on the applied electric field, the kind of incident particle and the energy. To get a MOSFET detector with a more lineal and sensible behaviour a positive bias will be applied at the gate during the radiation to prevent the immediate electron – hole recombination and causing an increment in the hole trapping efficiency.

However MOSFET detectors present some issues making the measurements:

- SiO_2 layer: is the detector’s acting volume, it usually has the dimensions 0.2×0.2 mm² being the oxide width around 200 – 800 Å. If this width is increased the number of electron – hole pairs generated in the oxide will also be increased, and so will the sensibility of the detector. The problem is that the oxide layers are very wide ($\geq 1\mu m$) and they required growth times of just about 100 hours at temperature of 1000°C. This is not economically feasible.
- Interface of radiation produced states: MOSFET radiation will increase trap’s density in the SiO_2 – Si alongside the increment of positive charge in the oxide. This phenomenon will make the threshold voltage change to a higher value, which will have two contributions, the one from the holes trapping; and the one from the charge states in the trap’s interface.

- Data acquisition and analysis techniques: a lot of MOSFET only operate in integral mode which limits the applications of these detectors in situations in which the radiation's fluence varies with time.
- Temperature effect: temperature effects in the detector have to be evaluated for in vivo dosimetry, given that the MOSFET is in direct contact with the human body ($T \simeq 37^\circ\text{C}$) while it's measuring. Studies show that temperature effect in measurements is small ($0.3\%/^\circ\text{C}$) for p - type MOSFET detectors at $T \simeq 22 - 40^\circ\text{C}$, and its sensibility doesn't depend on the temperature.
- Finite half - life: the biggest limitation of MOSFET detectors is its finite half - life, caused by saturation of the holes traps near the $\text{SiO}_2 - \text{Si}$ interface as the dose increases. This saturation reaches a point where there is not observable change in the threshold voltage and the detector cannot make correct measurements.

4.3 Clinical application of MOSFET in HDB

One of the advantages of MOSFET detectors over standard semiconductor devices for radiation detection, which are based on the collection of the charge produced by the ionizing radiation, is that they can be built in a very small size (microMOSFETs), and in recent times it has been developed a miniature MOSFET linear array that can be seen in Figure 9. This MOSFET linear array allows the measurement of the distribution of the dose radiation from the localization of the tumor to the position where the array is placed.



Figure 9: This figure shows a MOSFET linear array, in which the five MOSFET detectors are separated by a orange and white plastic [20].

In a recent paper [21] it was studied the MOSFET radial dose rate distributions of a HDR ^{192}Ir source in water and compared the results with Monte Carlo simulations. The conclusion was that MOSFET detectors could be used for absolute dose measurement, even in the vicinity of ^{192}Ir source, with appropriate calibration and correction, but the main limitation is its relatively large volume for *in vivo* dosimetry. That is the reason a new MOSFET was introduced, a miniature MOSFET or microMOSFET detector that can be inserted into a brachytherapy catheter.

MOSFET detector are perfect for brachytherapy for the following reasons:

- small detector size (microMOSFET)
- isotropic angular response
- fits inside brachytherapy catheters
- anatomical localitations
- available as a single detector or as a five – detector – array

The simulations made in this work and shown in section 6 and can to be contrasted with the precise measurements carried out by the new MOSFET used in quality control of the dose absorbed by the OARs in brachytherapy.

5 Radiation theory

The magnitude that will be studied in this work is the *absorbed dose rate* for a specific source and material. This magnitude is defined as

$$\dot{D} = \dot{\Psi} \frac{\mu_{en}}{\rho}, \quad (1)$$

where is $\dot{\Psi}$ the energy fluence rate incident on the material, measured in Jm^{-2} , and $\frac{\mu_{en}}{\rho}$ is the mass energy absorption coefficient of that material for a given photon energy, measured in $m^2kg^{-1}s^{-1}$. It is related to the total cross section of photon interaction, which is a sum of all contributions from the principal photon interactions: atomic photoeffect, Rayleigh and Compton scattering, electron-positron production and photonuclear [22]. As stated in [23], the energy fluence is a way to express the instantaneous rate of energy flow per unit area and per unit time, and it only depends on the radiation source, not on the material in which is measured. On the other hand, the mass energy absorption coefficient only depends on the material in which is being measured and on the energy of the photons used as radiation, in addition it is a known quantity and the values for elemental media, compounds and mixtures as a function of photon energy can be found in [22].

Another magnitude that has been presented in the introduction is the kinetic energy released or *kerma*, which is the sum of all initial kinetic energies of all of the charged particles that have been freed by uncharged ionizing particles in a material per unit mass. Kerma and absorbed dose may seem the same, but they are not, while kerma measures ions created in some material because of the radiation; absorbed dose measures the ions that are absorbed back into the material in which they are created.

The kerma dose rate is defined as

$$\dot{K} = \dot{\Psi} \frac{\mu_{tr}}{\rho}, \quad (2)$$

where $\frac{\mu_{tr}}{\rho}$ is the mass energy attenuation coefficient, which describes the amount of energy transferred to a material for a given energy photon. This parameter takes into account the escape of only secondary photon radiations produced at the initial photon-atom interaction and from the annihilation of positrons. It has been found that the kerma and the mass-energy attenuation coefficient $\frac{\mu_{tr}}{\rho}$ offer a clearer understanding of the methods used to calculate the mass energy-absorption coefficient $\frac{\mu_{en}}{\rho}$ [22].

As can be seen these two magnitudes are pretty similar, in fact, there is a situation in which they are equal, charged particle equilibrium (CPE), when the sample is very thin. Because of this they can be considered equivalent.

To be able to create a suitable radiation treatment plan for the patient, medical physicists need to be aware of a series of data, among which is the absorbed dose rate of brachytherapy in the tissue that is going to be radiated. The problem is that a direct measurement of absorbed dose or kerma is almost impossible, and quite difficult. The solution is to measure kerma and absorbed

dose on air for the desired radioactive source and then extrapolate those results to the material in which the radiation is absorbed, for example, hyaluronic acid or adipose tissue in the case of our simulation. The kerma of a source in air is called air kerma, and is defined as the kerma per unit mass of air. Another problem that is faced is that air kerma cannot be measured directly either; what can be measured is the air kerma strength (S_k) of a source, which is defined as the air kerma rate at the point along the transverse axis of the source in free space, and gives a measurement of the brachytherapy source strength, as stated in [25]. This magnitude is defined as the product of air kerma rate at a calibration distance d , multiplied by the square of that distance.

$$S_k = \dot{K} d^2 \quad (3)$$

This magnitude S_k has units of unit of air kerma strength (U), which is related to units of time, kerma and distance in the following way:

$$1U = 1 \frac{\mu Gy m^2}{h} = 1 \frac{cGy cm^2}{h}$$

Another way to define absorbed dose rate for a point source is using the inverse square law, assuming that $\mu_{en} \simeq \mu_{tr}$

$$\dot{D} = \frac{\Gamma A(t)}{r^2}, \quad (4)$$

being Γ the gamma rate dose constant, defined as $\Gamma = \frac{S_k}{A(t)}$, which is characteristic of each radionuclide, measured in $\frac{Gy cm^2}{s Bq}$; $A(t)$ the activity of the radionuclide used in Bq and r linear thickness used to measure in cm .

As can be seen the gamma rate dose constant, Γ is related to the air kerma strength S_k by the activity of the radionuclide. It can also be defined as a sum over the number gamma rays emitted by the radionuclide of energy E_i with probability P_i , as shows [24].

$$\Gamma = \frac{1}{4\pi R^2} \sum P_i h(E_i), \quad (5)$$

where R is the distance to the source (100 cm), P_i is the emission probability of each gamma ray, E_i is the energy of each gamma ray in MeV, and $h(E_i)$ is the dose rate flux per unit density or fluence. To obtain the relation between fluence and dose for γ rays and neutrons the following expression should be computed [26]

$$h(E) = 10^{-12} e^{A+BX+CX^2+FX^3+GX^4}, \quad (6)$$

where $h(E)$ is the fluence-to-dose factor, measured in $Sv cm^{-2}$ expressed as an analytical function of energy E , measured in MeV, and X the natural logarithm of the energy ($\ln E$). The values of the coefficients for γ rays can be found

in [26].

The gamma rate dose constant allows the calculation of exposure rate for a point source, for a given activity, at a specific distance from the source and of a gamma – emitting radionuclide. It is typically measured in R/h at 1 m for a 1Ci source.

Gamma rate dose constants for several radionuclides have been obtained from [24]. The equivalences from the Γ given in [24] and the ones used in the simulation are shown in Table 1. To be able to obtain these equivalences it is compulsory to know how to change units. This is shown in the Introduction.

Isotope	$\Gamma(\frac{mSv m^2}{h MBq})$	$\Gamma(\frac{Gy cm^2}{s Bq})$
^{192}Ir	$1.599 \cdot 10^{-4}$	$3.33 \cdot 10^{-13}$
^{137}Cs	$1.032 \cdot 10^{-4}$	$2.86 \cdot 10^{-13}$
^{133}Ba	$1.231 \cdot 10^{-4}$	$3.42 \cdot 10^{-13}$
^{133}Xe	$2.783 \cdot 10^{-5}$	$7.73 \cdot 10^{-14}$
^{60}Co	$3.703 \cdot 10^{-4}$	$1.03 \cdot 10^{-12}$

Table 1: This table shows the values of Γ in $\frac{mSv m^2}{h MBq}$ given in [2], and in $\frac{Gy cm^2}{s Bq}$ used in the simulation for all the radionuclide used (^{60}Co , ^{133}Xe , ^{133}Ba , ^{137}Cs , ^{192}Ir).

For a given gamma source emitting several photons at different energies and with different probabilities, the average attenuation coefficient is obtained computing the thickness t of the material required for 95% attenuation

$$0.05\Gamma = \sum \Gamma_i e^{\mu(E_i)t},$$

where μ is the attenuation coefficient in cm^{-1} on the corresponding E_i energy and in the corresponding material (water, biological tissue, HA).

The value of t has been determined by an iterative procedure, and the value of the mean attenuation coefficient, $\langle \mu \rangle$ has been determined by solving the following equation for μ :

$$0.05 = e^{-\langle \mu \rangle t} \quad (7)$$

The values obtained for the mean attenuation coefficient for the radionuclides studied in the simulation have been obtained using a MatLab program (which is shown in Appendix 2) can be seen in Table 2.

When the attenuation μ is taking into consideration the expression studied of the absorbed dose rate $\dot{D} = \frac{\Gamma A}{r^2}$ changes to

$$\dot{D} = \frac{\Gamma A}{r^2} e^{-\langle \mu \rangle r}, \quad (8)$$

Isotope	$\mu_{H_2O} (cm^{-1})$	$\mu_{HA} (cm^{-1})$	$\mu_{AT} (cm^{-1})$
^{192}Ir	0.1069	0.128	0.1017
^{137}Cs	0.0870	0.0870	0.0827
^{133}Ba	0.1422	0.1734	0.1344
^{133}Xe	0.2703	0.2323	0.2703
^{60}Co	0.0632	0.0601	0.0632

Table 2: This table shows the average linear attenuation coefficient for each radionuclide for water, hyaluronic acid and adipose tissue.

which is the expression that will be used in the simulation. There are two effects included in this equation, the first one is purely geometrical (the $\frac{1}{r^2}$ factor) and the second one takes into account the energy transfer to the medium, $e^{<-\mu>r}$.

5.1 Attenuation produced by a Hyaluronic Acid layer

In this section the relative absorption produced by a width r for a collimated beam of monoenergetic photons is studied.

From [27] an expression that connects the attenuation of hyaluronic acid and water has been found

being

$$\chi = \frac{\frac{\mu_{HA}}{\rho_{HA}}}{\frac{\mu_{H_2O}}{\rho_{H_2O}}}$$

the ratio between the mass attenuation coefficient for water and HA the equivalence can be expressed as

$$\mu_{HA} = \chi \frac{\rho_{HA}}{\rho_{H_2O}} \mu_{H_2O} = \chi \mu_{H_2O}, \quad (9)$$

where μ is the linear attenuation coefficient and ρ the density of the corresponding material. The equivalence stated in Eq. (9) is only correct when the density of water and HA is considered the same.

Given that one of the purpose of this work is to study the change in absorbed dose rate in OARs when a hyaluronic acid layer is placed between the rectum and the prostate, absorption must be studied. In [27] the absorption is defined as the fraction of the incident radiation, I_0 , that is interacts within a material of linear thickness r ; in other words, is the fraction of the incident radiation that cannot reach the OAR. For a given energy of the photon, the absorption produced by the material used in the layer, in our case hyaluronic acid (HA) can be compared with the one produced by water for the same linear thickness, using the equivalence between their mass coefficient attenuation and the exponential attenuation law

$$I(r) = I_0 e^{-\mu_{mat} r} \quad (10)$$

For a collimated beam of monoenergetic photons coming from a infinite distance, and taking into account Eq. (9), the relative absorption produced by a width r is given by

$$A(r) \equiv \frac{I_0 - I(r)}{I_0} = (1 - e^{-\mu_{HA} r}) = (1 - e^{-\mu_{H_2O} r}) \simeq \mu_{HA} r = \chi \mu_{H_2O} r, \quad (11)$$

assuming that $(\mu_{HA} r) \ll 1$, which is a realistic approximation taking into account the widths used in the protection of the OARs.

Conversely, if the finite distance effects are contemplated, as is the case of a brachytherapy treatment, the geometrical $\frac{1}{r^2}$ has a great influence that needs to be analyzed. The inclusion of a shell of width Δr of HA, will produce an attenuation shown in the following expression

$$A(r, \Delta r) = \frac{I(r) - I(r, \Delta r)}{I(r)} = 1 - \left[\frac{1}{1 + (\frac{\Delta r}{r})^2} \right] e^{-\mu_{HA} \Delta r}, \quad (12)$$

where is being considered an isotropic propagation in two portions of homogeneous media, with linear attenuation coefficients μ_0 and μ_{HA} . For a point – like source of intensity S_0 , the intensities at the points r and $r + \Delta r$ are given by

$$I(r) = \frac{S_0}{4\pi r^2} e^{-\mu_0 r} \quad (13)$$

$$I(r, \Delta r) = \frac{S_0}{4\pi(r + \Delta r)^2} e^{-\mu_0 r} e^{-\mu_{HA} \Delta r} \quad (14)$$

In the actual simulations S_0 is taken from Eq. (8) as $S_0 = 4\pi\Gamma A(t)$.

To fully comprehend the geometry of the HA layer and the intensity at points r and $r + \Delta r$ a scheme has been provided in Figure 11.

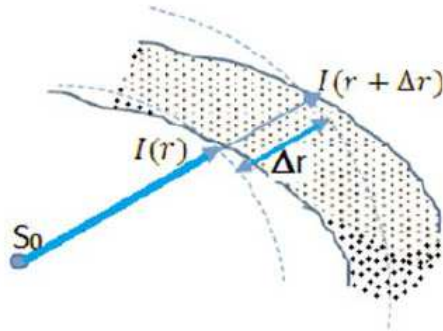


Figure 10: This figure shows Scheme of the geometry of the HA shell, indicated by the dotted region, used to calculate the intensities due to the source S_0 as given by Eq. (13) and Eq.(14).

Taking Eq. (13) and Eq. (14) in the expression of Eq. (12) the change of the absorption with the geometry can be studied. There are three situations:

1. $\frac{\Delta r}{r} \ll 1$: the source is at a long distance from the OAR

$$A(r, \Delta r) \simeq 2\frac{\Delta r}{r} + \mu_{HA}r + \dots \quad (15)$$

2. $\Delta r \approx r$: the distance from the source to the OAR is equivalent to the width of the shell

$$A(r, \Delta r) \simeq \frac{3}{4} + \frac{1}{4}\mu_{HA}r + \dots \quad (16)$$

3. $\frac{\Delta r}{r} \gg 1$: the source is at a very short distance from the OAR

$$A(r, \Delta r) \simeq 1 - \left(\frac{r}{\Delta r}\right)^2 + \mu_{HA}\Delta r \left(\frac{r}{\Delta r}\right)^2 + \dots \quad (17)$$

6 Simulations

The purpose of this work is to study the absorbed dose rate at the organs at risk (OAR) in a brachytherapy treatment for prostate cancer. This study will be made in two cases, the first one when there is no protection between the rectum walls and the prostate, and the second one when an hyaluronic acid layer is placed between the rectum and the prostate, as indicated in Figure 11 .

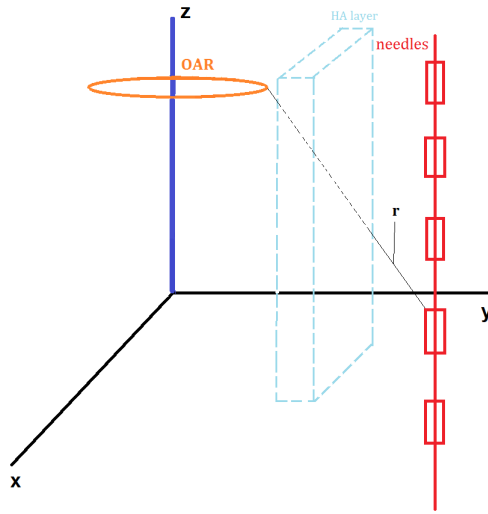


Figure 11: This figure shows the representation of the real system used in a brachytherapy technique, where there is the organ at risk in which the absorbed dose is studied, the HA layer that serves as protection, the needles, inside of which is the radioactive source, showing the different positions it has in the walkthrough, as well as the distance between a position of the needle and the OAR r .

6.1 Geometrical parameters

The main result to perform the calculations is given by Eq. (8), Eq. (13) and Eq. (14).

The first step of this simulation is to study the anatomy of the male reproductive system and its geometry, to be able to build a realistic model. This step is one of the most important of this work, given that if the geometry is not studied correctly the results obtained, once the absorbed dose rate is calculated, will be wrong. In Figure 5, it can be seen that the prostate (approximated diameter 5 cm) lays below the bladder, above the penis and in front of the rectum. It is crossed by the urethra, which connects the bladder and the penis, as can be seen in Figure 12.

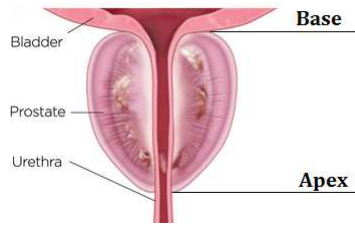


Figure 12: This figure shows in a more detailed way the position of the prostate, the bladder and the urethra, including the base and the apex [29].

Once the geometry of the anatomy of the male reproductive system is studied and understood the simulation can be made. The proposed geometry is displayed in Figure 13.

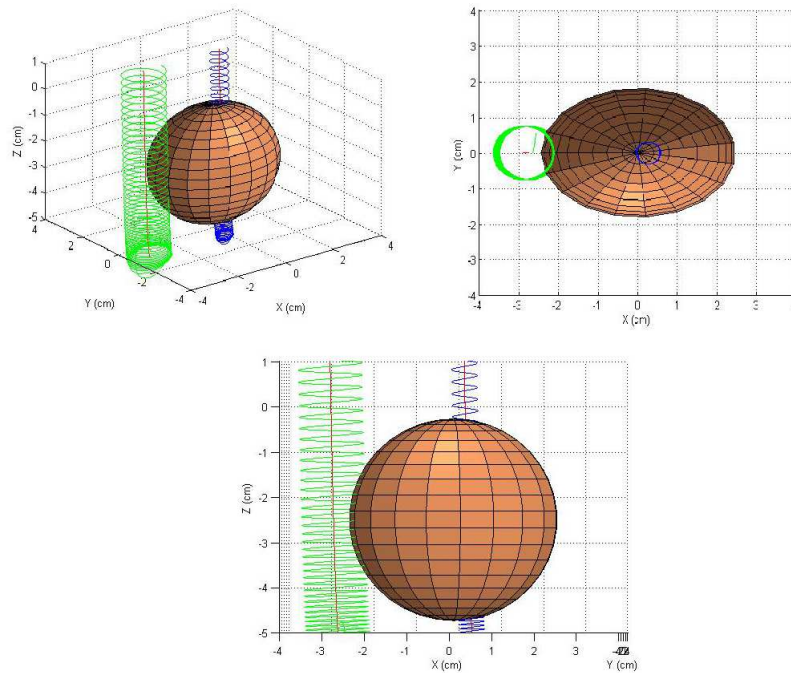


Figure 13: This figure shows shows the simulation obtained for the geometry of the prostate, rectum and urethra in three perspectives, up left is the 3D perspective, up right is the perspective in the YX plane, and down is the ZY plane perspective. The brown ellipsoid represents the prostate with an approximated diameter of 5 cm; the green cylinder at its left represents the rectum; and the blue cylinder represents the urethra, which crosses the prostate.

In the brachytherapy treatment studied in this simulation a series of hollow needles are inserted, as can be seen in Figure 14. Inside these needles is the radioactive source that will deliver the desired radiation to kill the cancer cells

and get rid of the tumor. The seeds are moved along the needles performing several programmed stops with its corresponding time, that can be the same one for all pauses or can be different. One of the aspects that have to be studied in the treatment planning is the number of the pauses, the positions and the time the source will be in each position. These parameters will depend on a large number of factors, but the more significant ones will be the placement and the size of the tumor. The needles used in the simulation studied in this work have a longitude of 30 cm, and the number of pauses, as well as the time and geometry have been taking from a real treatment.

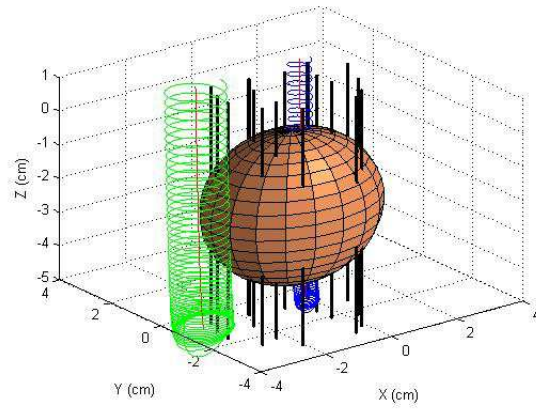


Figure 14: This figure shows the prostate, rectum and urethra, as well as the 16 needles used in the brachytherapy treatment in a 3D perspective.

6.2 Dose at OARs without HA protection

In a brachytherapy treatment the main source put inside the needles is ^{192}Ir , but in this work we have studied other isotopes, and we have compared the results obtained. The absorbed dose has been examined on the walls of the urethra and on the walls of the rectum. This dose is going to be a function of the duration of the programmed stops for the seeds, and the expression of the dose as a function of time can be obtained from Eq. (8).

$$D = \dot{D} \Delta t = \frac{\Gamma A(t)}{r^2} e^{-\langle \mu \rangle r} \Delta t \quad (18)$$

In Figure 15 can be seen the results obtained for the absorbed dose rate on the walls of the urethra for the five isotopes used in this simulation, ^{192}Ir , ^{137}Cs , ^{133}Ba , ^{133}Xe and ^{60}Co .

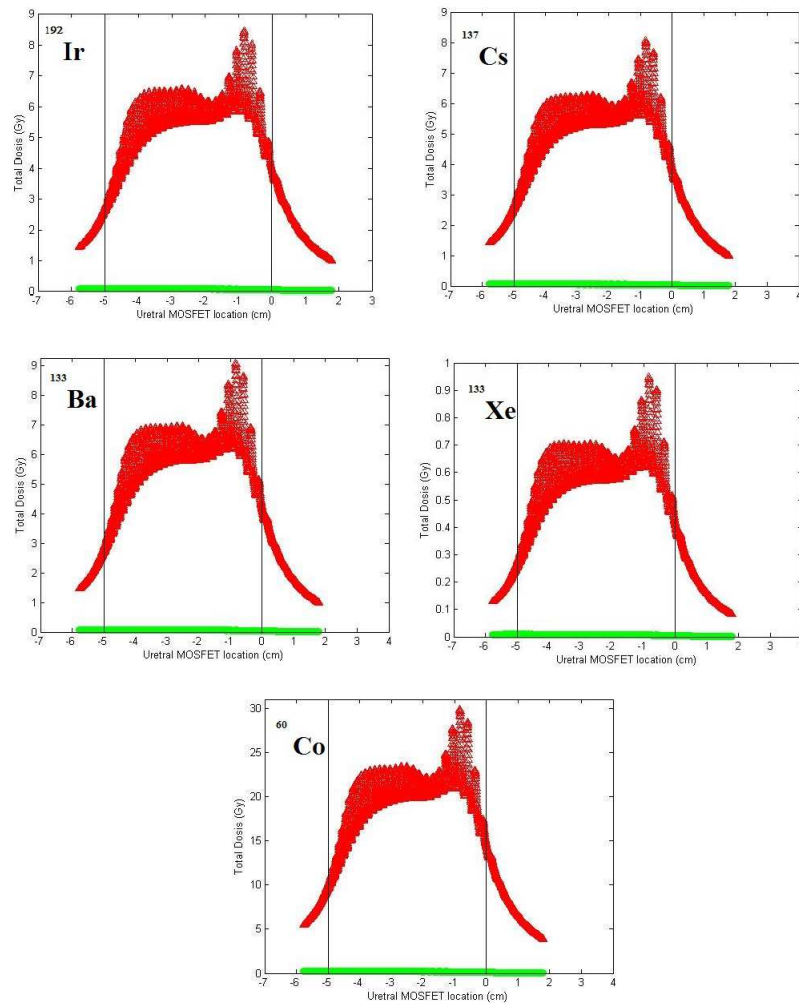


Figure 15: This figure shows the total absorbed dose rate in the walls of the urethra in Gy for the different isotopes used in the simulation as a function of the longitude of the urethra. Each graph shows the name of the corresponding isotope and it also shows the limits of the prostate by two vertical lines. The red graph is the dose caused by all the stops of the treatment, while the green one is caused by the way in and way out of the seed inside the needles.

The results obtained in these simulations are feasible, given that the highest dose is in the middle of the prostate where is needed to treat the cancer. The highest dose is not exactly in the middle of the prostate, given that it has a peak at the base of the prostate, caused by a larger stop time of the seeds. At the base of the prostate a larger stop time is needed, because there are less seeds' stops contributing to the dose when compared to the number of stops in the middle of the prostate; and to obtain the same dose gotten in the middle of the prostate a larger stop time is needed at the beginning of it. However, and as far as we are using a realistic treatment, it can be seen that depending

on the radioisotope the total dose changes, which is normal, given that each radioisotope has a different gamma constant, as was obtained in the previous chapter, and it affects the dose.

Aforementioned that two cases were to be studied, one in which there would be no protection between the prostate and the rectum; and one where the protection would be an HA layer. As can be deduced the absorbed dose rate on the walls of the urethra for these two cases will be the same, and that is the reason they had been studied apart.

The total absorbed dose rate on the walls of the rectum on the first case (with no protection) can be seen in Figure 16. These values can be experimentally checked using the microMOSFET dosimeters described in section 4.2.

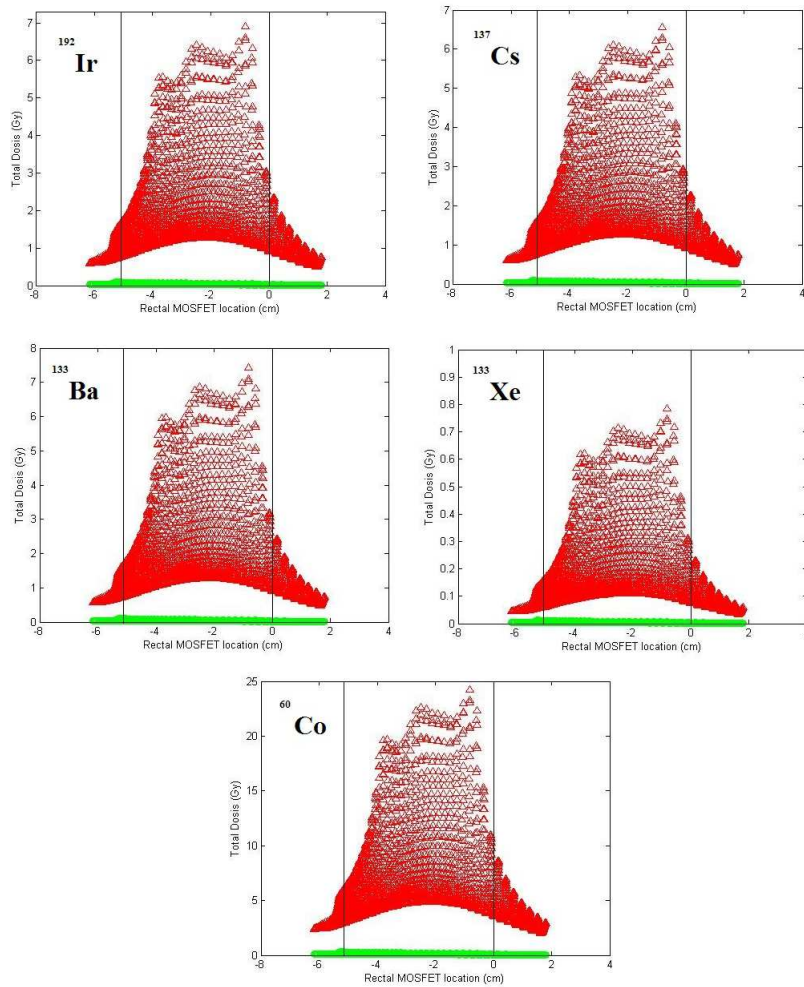


Figure 16: This figure shows the total absorbed dose rate in the walls of the rectum in Gy for the different isotope used in the simulation as a function of the longitude of the rectum when there is no protection between the prostate and the rectum. Each graph shows the name of the corresponding isotope and it also shows the limits of the prostate by two vertical lines. The red graph is the dose caused by all the stops of the treatment, while the green one is caused by the way in and way out of the needles.

As it happened with the dose on the urethra the highest dose is found in the middle of the prostate, with a small peak at the beginning of it. It may seem that it has a strange shape, but the dose has been calculated in the entire wall of the rectum, so lower absorbed dose corresponds to the rear part of the rectum wall, while the higher absorbed dose corresponds to the front part of the rectum wall.

The results of our simulation for ^{192}Ir presented in Figure 16 are in good

agreement with the results from the real treatment.

6.3 Effect of the HA layer

The use of an HA layer is to verify its usefulness as a protection against radiation. The insertion of a HA layer with a width of 1.5 cm will change the geometry of the rectum and the prostate, as was sketched in Figure 11 and can be viewed in Figure 17.

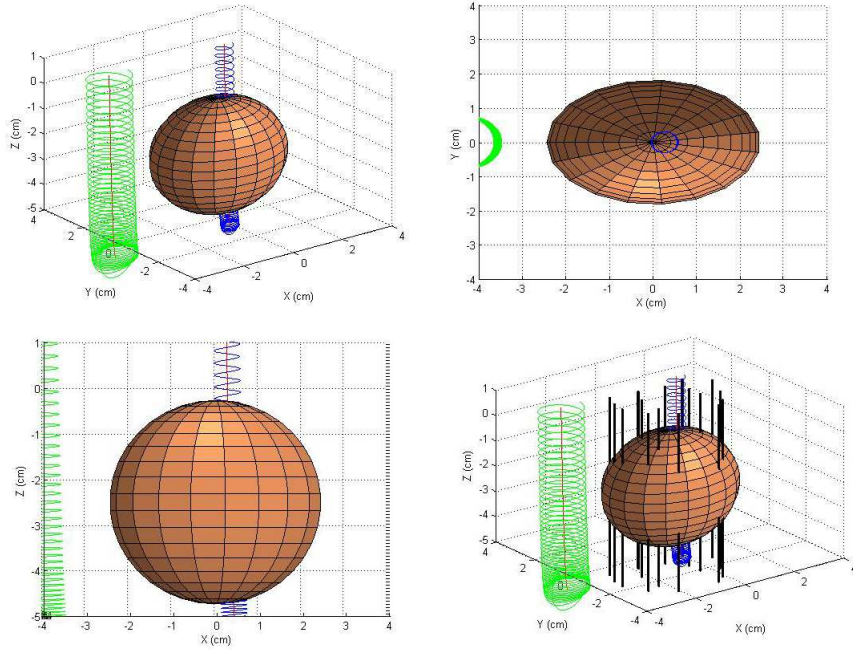


Figure 17: This figure shows the geometry of the prostate (brown ellipses), the rectum (green cylinder) and the urethra (blue cylinder) when a HA layer of 1.5 cm has been introduced between the prostate and the rectum walls. There are three perspectives, up left is the 3D perspective of the rectum, the urethra and the prostate; up right is the YX plane perspective; down left is the ZX plane perspective; and down right is the 3D perspective of the rectum, the urethra, the prostate and the needles used in the treatment.

Before the results of the calculated absorbed dose in the walls of the rectum when a layer of HA is used as protection are presented, an estimation of the obtained reduction is performed using the expression of the attenuation and intensities from Eq. (12), Eq. (13) and Eq. (14). Supposing the diameter of the rectum is 5 cm, which results in an average distance from the source to the rectum walls of $r = 5 + 2.5 = 7.5$ cm, and the width of the HA layer $\Delta r = 1.5$ cm, the results obtained using the different estimations for the absorption given by Eq. (15) and Eq. (16) are:

- The attenuation of the farthest rectum walls when there is protection in the form of a HA layer, taking the values of the average linear attenuation coefficient from Table 2 is

$$A(r, \Delta r) \simeq 2 \frac{\Delta r}{r} + \mu_{HA} r = 60\%$$

- The attenuation of the closest rectum walls when there is protection in the form of a HA layer, taking the values of the average linear attenuation coefficient from Table 2 is

$$A(r, \Delta r) \simeq \frac{3}{4} + \frac{1}{4} \mu_{HA} r = 95\%$$

These results have been obtained for the ^{192}Ir source, but the influence of the average linear attenuation coefficient is not the dominant one in the results.

This estimations are in agreement with the results obtained from the comparison of the calculated values give in Figures 16 and 18.

Now the results for the total absorbed dose rate on the walls of the rectum when a layer of 1.5 cm of HA has been introduced obtained through the simulation can be observed in Figure 18.

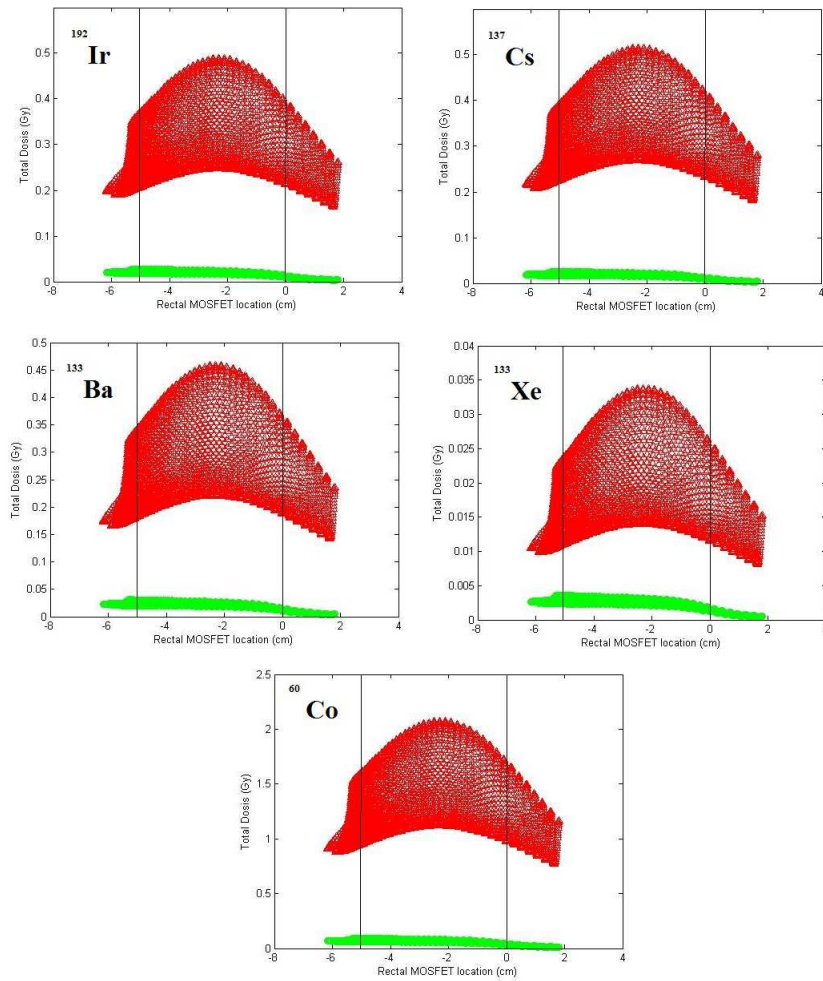


Figure 18: This figure shows the total absorbed dose rate in the walls of the rectum in Gy for the different isotope used in the simulation as a function of the longitude of the rectum when a protection in the form of a 1.5 cm HA layer has been introduced between the prostate and the rectum. Each graph shows the name of the corresponding isotope and it also shows the limits of the prostate by two vertical lines. The red graph is the dose caused by all the stops of the treatment, while the green one is caused by the way in and way out of the radioactive seeds.

7 Conclusions

The purpose of this work was to evaluate in a realistic way through a simulation the absorbed dose of the organs at risk (OAR) in a brachytherapy treatment for prostate cancer and calculate the protection effect of a layer of hyaluronic acid. Prostatic cancer affects almost 15% of men and causes the death of 13% of them. Our study enlightens the difficulty of protecting the organs at risk in the treatment of this disease, in particular the urethra.

1. We have described the physical basis of microMOSFET dosimeters, which are the necessary tools to control the radioactive dose in some OARs.
2. The male anatomy of the reproductive system has been examined to have the capacity of creating a mathematical model of its geometry and be able to make a simulation of it using MatLab.
3. The principal goal was to study the protection effect of the hyaluronic acid layer. This effect was proven true when the absorbed dose on the walls of the rectum without the protection (Figure 16) was one order of magnitude greater than the absorbed dose there with protection (Figure 18). When a comparison between the results presented in Figure 16 and the ones presented in Figure 18 is made, it is safe to say that placing a layer of HA as protection reduces considerably the total absorbed dose, approximately between 60% and 90% of the dose is attenuated, which is in agreement with approximate estimations. These results correspond to a ^{192}Ir source, but as far as they are mostly dominated by the geometry equivalent results are expected for other sources.
4. In addition to this goal the absorbed dose in the urethra has been calculated, and it opens a gate to future studies on the protection of this organ, such as the use of different radiation sources.
5. Even though the most used radioactive source is ^{192}Ir , the simulation has been made with four more radionuclides, with different outcomes. For ^{137}Cs the absorbed dose is slightly smaller than the one obtained for ^{192}Ir , while for ^{133}Ba is slightly bigger. However, for ^{133}Xe is several orders of magnitude smaller, which would make it a perfect candidate to replace the ^{192}Ir as go-to-source in therapies, but the problem is that it is a noble gas and its handling is pretty difficult. On the other hand ^{60}Co shows a much bigger absorbed dose due to the higher energy of the emitted photons, which is one of the reasons it was replaced with ^{192}Ir .
6. Our results, which used the parameters extracted from the data of a real treatment, can be checked using the standard simulation procedures in the brachytherapy and also by means of dose measurements performed with microMOSFET.

References

- [1] ICRU, *Fundamental Quantities And Units For Ionizing Radiation (Revised)*, Volume 11 N°1 (2011)
- [2] Defender Shield, *Damaging Effects of EMF Exposure on a Cell*,
URL: <https://www.defendershield.com/damaging-effects-emf-exposure-cell/>
- [3] National Cancer Institute (NIH), *Radiation Therapy for Cancer*, (June, 30, 2010),
URL:<http://www.cancer.gov/about-cancer/treatment/types/radiation-therapy/radiation-fact-sheet>
- [4] Cancer Research UK, *General side effects of radiotherapy*, (March, 14, 2016),
URL:<http://www.cancerresearchuk.org/about-cancer/cancers-in-general/treatment/radiotherapy/side-effects/general/radiotherapy-reactions>
- [5] Zhen Yu Qi, *Mosfet dosimetry in HDR brachytherapy and IMRT for nasopharyngeal*, Research Online, University of Wollongong, (2010)
- [6] National Cancer Institute, SEER Training Modules, *Type of Radiation Therapy*,
URL: <http://training.seer.cancer.gov/treatment/radiation/types.html>
- [7] Gobierno de España, *REAL DECRETO 815/2001, de 13 de julio, sobre justificación del uso de las radiaciones ionizantes para la protección radiológica de las personas con ocasión de exposiciones médicas. BOE nº 168 14/07/2001*,
URL: <http://www.insht.es/portal/site/Insht/menuitem.1f1a3bc79ab34c578c2e8884060961ca/?vgnext=b67d7253801d5110VgnVCM10000dc0ca8c0RCRD&vgnextchannel=f3cc6b33a9f1110VgnVCM10000dc0ca8c0RCRD&tab=tabConsultaCompleta>
- [8] Gobierno de España, *Real Decreto 783/2001, de 6 de julio, por el que se aprueba el Reglamento sobre protección sanitaria contra radiaciones ionizantes*.
URL: https://www.boe.es/diario_boe/txt.php?id=BOE-A-2001-14555
- [9] Nucleonica wiki, *Dosimetry and Shielding*,
URL: <http://www.nucleonica.net/wiki/index.php?title=Help%3ADosimetry%26Shielding%2B%2B>
- [10] Nicholas G. Zaorsky, Timothy N. Showalter, Gary A. Ezzell, Paul L. Nguyen, et al, *External Beam Radiation Therapy Treatment Planning For Clinically Localized Prostate Cancer*, American College of Radiology, (2016)
- [11] Mayo Clinic, *Slide show: Radiation therapy treatment planning*, (2015)
URL:<http://www.mayoclinic.org/diseases-conditions/cancer/multimedia/radiation-therapy/sls-20076358?s=1>

- [12] Radiation Oncology Victoria, *Stereotactic Radiotherapy*, (2013), URL: <http://www.radoncvic.com.au/for-patients/what-to-expect/stereotactic-radiotherapy>
- [13] Prada, P. J., Fernández, J., Martínez, A. A., la Rúa, de, Á., Gonzalez, J. M., Fernandez, J. M., and Juan, G. , *Transperineal Injection of Hyaluronic Acid in Anterior Perirectal Fat to Decrease Rectal Toxicity From Radiation Delivered With Intensity Modulated Brachytherapy or EBRT for Prostate Cancer Patients*, *Int. J. Radiat. Oncol. Biol. Phys.*, 2007; 69(1), 95–102. doi:10.1016/j.ijrobp.2007.02.034
- [14] OzRadOnc, *11.10.9 - In Vivo Dosimetry*, URL:<http://ozradonc.wikidot.com/in-vivo-dosimetry>
- [15] American Association for Cancer Research (AACR), *Prostate Cancer Treatment (PDQ®)*, URL: <https://www.aacrfoundation.org/CancerTypes/Pages/PDQs/Prostate-Cancer-Treatment-PDQ.aspx#General-Information-About-Prostate-Cancer>
- [16] Wikipedia, *MOSFET*, URL: <https://en.wikipedia.org/wiki/MOSFET>
- [17] Joanna E. Cygler, *MOSFET applications in brachytherapy*, (December, 5, 2014)
- [18] Kron T, Rosenfeld A, Lerch M, Bazley S, *Measurements in radiotherapy beams using on-line MOSFET detectors*, *Radiat Prot Dosimetry*, (2002)
- [19] Crawford RH, *Mosfet in circuit design: Metal - Oxide - semiconductor field - effect transistors for discrete and integrated - circuit technology*, McGraw-Hill, New York, (1967)
- [20] Best Medical Canada, *Linear five MOSFET Array Dosimeter* Information brochure, (2016) URL: http://www.bestmedicalcanada.com/MOSFETs/linear5ive_array.pdf
- [21] Zilio VO, Joneja OP et al, *Absolute depth-dose-rate measurements for an ^{192}Ir HDR brachytherapy source in water using MOSFET*, *Med. Physics* (2006)
- [22] NIST: Physical Measurement Laboratory, *Tables of X-Ray Mass Attenuation Coefficients and Mass Energy-Absorption Coefficients from 1 keV to 20 MeV for Elements Z = 1 to 92 and 48 Additional Substances of Dosimetric Interest**, URL: <http://www.nist.gov/pml/data/xraycoef/>
- [23] Danielle R. Beaulieu, *Air Kerma Strength Measurement of a Cs-137 Radioisotope Using a Seven-Distance Ionization Technique and Comparison with the Gamma Spectroscopy Method*, A Major Qualifying Project Submitted to the Faculty of Worcester Polytechnic Institute (WPI), (2013)
- [24] Laurie M. Unger, D. K. Trubey, *Specific Gamma - Ray Dose Constants for Nuclides Important to Dosimetry and Radiological Assessment*, Oak Ridge National Laboratory (ORNL), Tennessee, (May, 1982)

- [25] Ravinder Nath, Lowell L. Anderson, Gary Luxton, Keith A. Weaver, Jeffrey F. Williamson, Ali S. Meigooni, *Dosimetry of Interstitial Brachytherapy Sources*, American institute of Physics, New York, (March, 1995)
- [26] American Nuclear Society (ANS), *Neutron and gamma-ray fluence-to-dose factors*, ANS, Illinois, (1991)
- [27] J. Sánchez Mazón, A. Mañanes Pérez, A. S. García Blanco, J. A. Vázquez Rodríguez, M. A. Mendiguren Santiago, P. J. Prada, *Measurement of the attenuation produced by Hyaluronic acid in the rectal protection during prostate cancer treatment with brachytherapy* (2016)
- [28] HyperPhysics, *Inverse square law*,
URL: <http://hyperphysics.phy-astr.gsu.edu/hbase/forces/isq.html>
- [29] Urology San Antonio,
URL: <https://www.urologysanantonio.com/wp-content/uploads/2015/11/Rezum-Prostate-BPH-Before-After.jpg>

Appendix: MATLAB programs

In this appendix the MATLAB programs that have been used in the simulation will be shown.

- **The attenuation coefficient**

```
%  
% Mass atenuation coefficients  
% and average mass atenuation coefficients  
%  
rhoWater=1.0;  
% Energía (MeV), mu/rho (cm^2/g), mu_en/rho (cm^2/g)  
DatosWater=[1.00000E-03 4.078E+03 4.065E+03  
1.50000E-03 1.376E+03 1.372E+03  
2.00000E-03 6.173E+02 6.152E+02  
3.00000E-03 1.929E+02 1.917E+02  
4.00000E-03 8.278E+01 8.191E+01  
5.00000E-03 4.258E+01 4.188E+01  
6.00000E-03 2.464E+01 2.405E+01  
8.00000E-03 1.037E+01 9.915E+00  
1.00000E-02 5.329E+00 4.944E+00  
1.50000E-02 1.673E+00 1.374E+00  
2.00000E-02 8.096E-01 5.503E-01  
3.00000E-02 3.756E-01 1.557E-01  
4.00000E-02 2.683E-01 6.947E-02  
5.00000E-02 2.269E-01 4.223E-02  
6.00000E-02 2.059E-01 3.190E-02  
8.00000E-02 1.837E-01 2.597E-02  
1.00000E-01 1.707E-01 2.546E-02  
1.50000E-01 1.505E-01 2.764E-02  
2.00000E-01 1.370E-01 2.967E-02  
3.00000E-01 1.186E-01 3.192E-02  
4.00000E-01 1.061E-01 3.279E-02  
5.00000E-01 9.687E-02 3.299E-02  
6.00000E-01 8.956E-02 3.284E-02  
8.00000E-01 7.865E-02 3.206E-02  
1.00000E+00 7.072E-02 3.103E-02  
1.25000E+00 6.323E-02 2.965E-02  
1.50000E+00 5.754E-02 2.833E-02  
2.00000E+00 4.942E-02 2.608E-02  
3.00000E+00 3.969E-02 2.281E-02  
4.00000E+00 3.403E-02 2.066E-02  
5.00000E+00 3.031E-02 1.915E-02  
6.00000E+00 2.770E-02 1.806E-02  
8.00000E+00 2.429E-02 1.658E-02  
1.00000E+01 2.219E-02 1.566E-02  
1.50000E+01 1.941E-02 1.441E-02  
2.00000E+01 1.813E-02 1.382E-02];  
%  
% lead (NIST)  
rhoPb=11.35; %densidad en g/cm^3  
  
% Energía (MeV), mu/rho (cm^2/g), mu_en/rho (cm^2/g)  
DatosPb=[1.00000E-03 5.210E+03 5.197E+03  
1.50000E-03 2.356E+03 2.344E+03  
2.00000E-03 1.285E+03 1.274E+03
```

2.48400E-03	8.006E+02	7.895E+02
2.48400E-03	1.397E+03	1.366E+03
2.53429E-03	1.726E+03	1.682E+03
2.58560E-03	1.944E+03	1.895E+03
2.58560E-03	2.458E+03	2.390E+03
3.00000E-03	1.965E+03	1.913E+03
3.06640E-03	1.857E+03	1.808E+03
3.06640E-03	2.146E+03	2.090E+03
3.30130E-03	1.796E+03	1.748E+03
3.55420E-03	1.496E+03	1.459E+03
3.55420E-03	1.585E+03	1.546E+03
3.69948E-03	1.442E+03	1.405E+03
3.85070E-03	1.311E+03	1.279E+03
3.85070E-03	1.368E+03	1.335E+03
4.00000E-03	1.251E+03	1.221E+03
5.00000E-03	7.304E+02	7.124E+02
6.00000E-03	4.672E+02	4.546E+02
8.00000E-03	2.287E+02	2.207E+02
1.00000E-02	1.306E+02	1.247E+02
1.30352E-02	6.701E+01	6.270E+01
1.30352E-02	1.621E+02	1.291E+02
1.50000E-02	1.116E+02	9.100E+01
1.52000E-02	1.078E+02	8.807E+01
1.52000E-02	1.485E+02	1.131E+02
1.55269E-02	1.416E+02	1.083E+02
1.58608E-02	1.344E+02	1.032E+02
1.58608E-02	1.548E+02	1.180E+02
2.00000E-02	8.636E+01	6.899E+01
3.00000E-02	3.032E+01	2.536E+01
4.00000E-02	1.436E+01	1.211E+01
5.00000E-02	8.041E+00	6.740E+00
6.00000E-02	5.021E+00	4.149E+00
8.00000E-02	2.419E+00	1.916E+00
8.80045E-02	1.910E+00	1.482E+00
8.80045E-02	7.683E+00	2.160E+00
1.00000E-01	5.549E+00	1.976E+00
1.50000E-01	2.014E+00	1.056E+00
2.00000E-01	9.985E-01	5.870E-01
3.00000E-01	4.031E-01	2.455E-01
4.00000E-01	2.323E-01	1.370E-01
5.00000E-01	1.614E-01	9.128E-02
6.00000E-01	1.248E-01	6.819E-02
8.00000E-01	8.870E-02	4.644E-02
1.00000E+00	7.102E-02	3.654E-02
1.25000E+00	5.876E-02	2.988E-02
1.50000E+00	5.222E-02	2.640E-02
2.00000E+00	4.606E-02	2.360E-02
3.00000E+00	4.234E-02	2.322E-02
4.00000E+00	4.197E-02	2.449E-02
5.00000E+00	4.272E-02	2.600E-02
6.00000E+00	4.391E-02	2.744E-02
8.00000E+00	4.675E-02	2.989E-02
1.00000E+01	4.972E-02	3.181E-02
1.50000E+01	5.658E-02	3.478E-02
2.00000E+01	6.206E-02	3.595E-02];

%

% Adipose Tissue (ICRU-44)

% Absorption edges for the constituent atoms are indicated by the atomic number and shell designation

% Z=11 Na K 1.07210E-03 2.182E+03 2.177E+03

% Z=16 S K 2.47200E-03 2.072E+02 2.060E+02

% Z=17 Cl K 2.82240E-03 1.420E+02 1.409E+02

rhoAT= 9.500E-01; % densidad en g/cm^3

% Energia (MeV), mu/rho (cm^2/g), mu_en/rho (cm^2/g)

```

DatosAdiposeTissue=[ 1.00000E-03  2.628E+03  2.623E+03
1.03542E-03  2.392E+03  2.387E+03
1.07210E-03  2.176E+03  2.171E+03
1.07210E-03  2.182E+03  2.177E+03
1.50000E-03  8.622E+02  8.601E+02
2.00000E-03  3.800E+02  3.787E+02
2.47200E-03  2.053E+02  2.043E+02
2.47200E-03  2.072E+02  2.060E+02
2.64140E-03  1.707E+02  1.696E+02
2.82240E-03  1.405E+02  1.396E+02
2.82240E-03  1.420E+02  1.409E+02
3.00000E-03  1.188E+02  1.178E+02
4.00000E-03  5.054E+01  4.983E+01
5.00000E-03  2.587E+01  2.531E+01
6.00000E-03  1.494E+01  1.446E+01
8.00000E-03  6.300E+00  5.917E+00
1.00000E-02  3.268E+00  2.935E+00
1.50000E-02  1.083E+00  8.103E-01
2.00000E-02  5.677E-01  3.251E-01
3.00000E-02  3.063E-01  9.495E-02
4.00000E-02  2.396E-01  4.575E-02
5.00000E-02  2.123E-01  3.085E-02
6.00000E-02  1.974E-01  2.567E-02
8.00000E-02  1.800E-01  2.358E-02
1.00000E-01  1.688E-01  2.433E-02
1.50000E-01  1.500E-01  2.737E-02
2.00000E-01  1.368E-01  2.959E-02
3.00000E-01  1.187E-01  3.194E-02
4.00000E-01  1.062E-01  3.283E-02
5.00000E-01  9.696E-02  3.304E-02
6.00000E-01  8.965E-02  3.289E-02
8.00000E-01  7.873E-02  3.211E-02
1.00000E+00  7.078E-02  3.108E-02
1.25000E+00  6.330E-02  2.970E-02
1.50000E+00  5.760E-02  2.839E-02
2.00000E+00  4.940E-02  2.610E-02
3.00000E+00  3.955E-02  2.275E-02
4.00000E+00  3.377E-02  2.050E-02
5.00000E+00  2.995E-02  1.891E-02
6.00000E+00  2.725E-02  1.773E-02
8.00000E+00  2.368E-02  1.612E-02
1.00000E+01  2.145E-02  1.509E-02
1.50000E+01  1.843E-02  1.365E-02
2.00000E+01  1.698E-02  1.293E-02];
% Tissue Soft (ICRU Four Component)
rhoTS=1.0; % densidad g/cm^3
% Energía (MeV), mu/rho (cm^2/g), mu_en/rho (cm^2/g)
DatosSoftTissue=[1.00000E-03  3.829E+03  3.818E+03
1.50000E-03  1.286E+03  1.283E+03
2.00000E-03  5.755E+02  5.736E+02
3.00000E-03  1.792E+02  1.781E+02
4.00000E-03  7.681E+01  7.598E+01
5.00000E-03  3.947E+01  3.880E+01
6.00000E-03  2.283E+01  2.226E+01
8.00000E-03  9.604E+00  9.163E+00
1.00000E-02  4.937E+00  4.564E+00
1.50000E-02  1.558E+00  1.266E+00
2.00000E-02  7.616E-01  5.070E-01
3.00000E-02  3.604E-01  1.438E-01
4.00000E-02  2.609E-01  6.474E-02
5.00000E-02  2.223E-01  3.987E-02
6.00000E-02  2.025E-01  3.051E-02
8.00000E-02  1.813E-01  2.530E-02
1.00000E-01  1.688E-01  2.501E-02

```

```

1.50000E-01  1.490E-01  2.732E-02
2.00000E-01  1.356E-01  2.936E-02
3.00000E-01  1.175E-01  3.161E-02
4.00000E-01  1.051E-01  3.247E-02
5.00000E-01  9.593E-02  3.267E-02
6.00000E-01  8.870E-02  3.252E-02
8.00000E-01  7.789E-02  3.175E-02
1.00000E+00  7.003E-02  3.073E-02
1.25000E+00  6.262E-02  2.937E-02
1.50000E+00  5.699E-02  2.806E-02
2.00000E+00  4.893E-02  2.582E-02
3.00000E+00  3.929E-02  2.258E-02
4.00000E+00  3.367E-02  2.044E-02
5.00000E+00  2.998E-02  1.894E-02
6.00000E+00  2.739E-02  1.785E-02
8.00000E+00  2.400E-02  1.638E-02
1.00000E+01  2.191E-02  1.546E-02
1.50000E+01  1.913E-02  1.420E-02
2.00000E+01  1.785E-02  1.360E-02 ];

```

```

%
%Gamma-Ray-Flux to Dose-Rate conversion factors
% ln(D(E)) = A + B x + C x^2 + F x^3

```

```

%
% x=ln(E) E in MeV
% Energy range (MeV) A B C F
CoefGRFtoDR=[ 0.01 0.03 -20.477 -1.7454 0.0 0.0
0.03 0.5 -13.626 -0.57117 -1.0954 -0.24897
0.5 5.0 -13.133 0.72008 -0.033603 0.0
5.0 15.0 -12.791 0.28309 0.10873 0.0 ];

```

```

%
% 60Co %ORLN may 1982
% Probability (%) Energy (keV) mu/rho-H2O mu/rho-AT mu/rho-Pb (cm2g-1)
Co60ProEn=[ 100 1173 0.0655 0.0656 0.0625
100 1333 0.0613 0.0614 0.0566
0.02 693.8 0.0844 0.0845 0.1079];

```

```

%
% 133Xe %ORLN may 1982
% Probability (%) Energy (keV) mu/rho-H2O mu/rho-AT mu/rho-Pb (cm2g-1)
Xe133ProEn=[ 13.64 30.6 0.3692 0.3023 29.3624
25.26 31 0.3649 0.2996 28.240
9.06 35 0.3219 0.2730 22.3400
0.22 79.6 0.1841 0.1803 2.4710
36.48 81 0.1830 0.1794 2.3554
0.07 177.7 0.1430 0.1427 1.4514];

```

```

%
% 133Ba
% Probability(%) Energy/keV mu/rho-H2O mu/rho-AdiposeT mu/rho-Pb (cm2g-1)
Ba133ProEn=[34.25 30.6 0.3692 0.3023 29.3624
63.42 31.0 0.3649 0.2996 28.7240
22.76 35.0 0.3219 0.2730 22.3400
2.14 53.1 0.2204 0.2077 7.1048
2.55 79.6 0.1841 0.1803 2.4710
32.97 81.0 0.1830 0.1794 2.3554
0.645 160.6 0.1476 0.1472 1.7987
0.44 223.1 0.1327 0.1326 0.8610
6.90 276.4 0.1229 0.1230 0.5436
17.79 302.8 0.1182 0.1184 0.3983
60.5 356.0 0.1116 0.1117 0.3075
8.67 383.8 0.1081 0.1082 0.2600];

```

```

%
% 133Ba
% Probability (%) Energy (KeV) mu/rho-Hyaluronic Acid HA (cm2g-1)

```

% measured values with two sigma error rho

rhoHA=1.0; % densidad g/cm^3

```
Bal133ProEnExpHA=[34.25 30.6 0.384 0.006
                  63.42 31.0 0.384 0.006
                  22.76 35.0 0.34 0.013
                  32.97 81.0 0.21 0.009
                   6.90 276.4 0.16 0.03
                  17.79 302.8 0.157 0.017
                  60.5 356.0 0.135 0.009
                   8.67 383.8 0.13 0.03];
```

%

%

% 137Cs %ORLN may 1982

% Probability (%) Energy (keV) mu/rho-H2O mu/rho-AT mu/rho-Pb (cm2g-1)

```
Cs137ProEn=[ 2.07 31.8 0.3563 0.2943 27.4472
             3.82 32.2 0.3520 0.2916 26.8088
             1.39 36.4 0.3069 0.2636 20.1056
             89.98 661.7 0.0862 0.0863 0.1371];
```

%

% 192Ir %ORLN may 1982

% Probability (%) Energy (keV) mu/rho-H2O mu/rho-AT mu/rho-Pb (cm2g-1)

```
Ir192ProEn=[ 1.13 61.5 0.2042 0.1961 4.8259
             1.95 63.0 0.2026 0.1948 4.6307
             0.84 71.4 0.1932 0.1875 3.5379
             0.47 201.3 0.1368 0.1366 0.9908
             3.29 205.8 0.1359 0.1358 0.9640
             0.26 283.3 0.1217 0.1217 0.5025
             0.73 374.5 0.1093 0.1094 0.2759
             3.16 484.6 0.0983 0.0984 0.1723
             0.4 489.1 0.0979 0.0980 0.1691
             0.08 423.1 0.1040 0.1041 0.2159
             2.64 65.1 0.2002 0.1930 4.3575
             4.52 66.8 0.1984 0.1915 4.1363
             1.97 75.7 0.1885 0.1837 2.9784
             0.183 136.34 0.1560 0.1551 2.9798
             28.67 295.96 0.1193 0.1194 0.4272
             30.0 308.46 0.1175 0.1176 0.3887
             82.81 316.51 0.1165 0.1166 0.3749
             0.664 416.47 0.1046 0.1047 0.2206
             47.83 468.07 0.0998 0.0999 0.1840
             4.515 588.58 0.0904 0.0905 0.1290
             8.23 604.41 0.0893 0.0894 0.1240
             5.309 612.47 0.0889 0.0890 0.1225
             0.2923 884.54 0.0753 0.0754 0.0812
             0.1 871.7 0.0758 0.0759 0.0824];
```

%

ProbIr=Ir192ProEn(:,1)/100.0; % probability

EnerIr=Ir192ProEn(:,2); % these energies are in keV

Mu00Ir=Ir192ProEn(:,3).*rhoWater; % Una de referencia calculada
previamente en Pb

Mu00ATIr=Ir192ProEn(:,4).*rhoAT; % Una de referencia calculada previamente
en AT

Mu00PbIr=Ir192ProEn(:,5).*rhoPb; %Valor calculado previamente (PublicaLinear) en
Pb

%

ProbBa=Bal133ProEn(:,1)/100.0; % probability

```

EnerBa=Ba133ProEn(:,2);           % these energies are in keV
Mu00Ba=Ba133ProEn(:,3).*rhoWater; % Valor calculado previamente en H2O
Mu00ATBa=Ba133ProEn(:,4).*rhoAT;  % Valor calculado previamente en Adipose
Tissue
Mu00PbBa=Ba133ProEn(:,5).*rhoPb; %Valor calculado previamente (PublicaLinear) en
Pb
%
ProbCo=Co60ProEn(:,1)/100.0; % probability
Enerco=Co60ProEn(:,2);           % these energies are in keV
Mu00Co=Co60ProEn(:,3).*rhoWater; % Una de referencia calculada previamente
en Pb
Mu00ATCo=Co60ProEn(:,4).*rhoAT;  % Una de referencia calculada previamente
en AT
Mu00PbCo=Co60ProEn(:,3).*rhoPb;  % Una de referencia calculada previamente
en Pb

%
ProbXe=Xe133ProEn(:,1)/100.0; % probability
EnerXe=Xe133ProEn(:,2);           % these energies are in keV
Mu00Xe=Xe133ProEn(:,3).*rhoWater; % Una de referencia calculada
previamente en Pb
Mu00ATXe=Xe133ProEn(:,4).*rhoAT;  % Una de referencia calculada previamente
en AT
Mu00PbXe=Xe133ProEn(:,3).*rhoPb;  % Una de referencia calculada previamente
en Pb

%
Prob=Cs137ProEn(:,1)/100.0; % probability
Ener=Cs137ProEn(:,2);           % these energies are in keV
Mu00=Cs137ProEn(:,3).*rhoWater;  % Una de referencia calculada previamente
en Pb
Mu00AT=Cs137ProEn(:,4).*rhoAT;   % Una de referencia calculada previamente
en AT
%Mu00PbCs=Cs137ProEn(:,3).*rhoPb; % Una de referencia calculada
previamente en Pb

%
%
%
EnerHABa=Ba133ProEnExpHA(:,2); % Energias experimentales para Ba y HA
Mu00HABa=Ba133ProEnExpHA(:,3).*rhoHA; % la medida experimental en el HA con E
de Ba
SigmaMu00HABa=Ba133ProEnExpHA(:,4); % Error en la medida previamente
[nEner, n2]=size(Ener); % número de energías diferentes que emite el isótopo
considerado

%hay que ir cambiando el Ba por los demás elementos aquí y arriba
%[nEnerCo, n2]=size(EnerIr); % cambiar Ba Ir
%[nEnerIr, n2]=size(EnerIr); % cambiar Ba Ir
%[nEnerBa, n2]=size(EnerIr); % cambiar Ba Ir
%[nEnerXe, n2]=size(EnerIr); % cambiar Ba Ir

[nEnerHABa, n2]=size(EnerHABa); % cambiar

% datos para Dose rate per unit flux density
DoseEE=0.0*Ener;
GammaEE=0.0*Ener;
LinearAttenuationEE=0.0*Ener;
E_D1=CoefGRFtoDR(:,1);
E_D2=CoefGRFtoDR(:,2);
C_A=CoefGRFtoDR(:,3);
C_B=CoefGRFtoDR(:,4);
C_C=CoefGRFtoDR(:,5);
C_F=CoefGRFtoDR(:,6);

```

```

%
% Tabla de referencia para coeficiente atenuacion masico
%
EnerMu=DatosWater(:,1);
% EnerMu=DatosPb(:,1); % atencion al material en MeV
% EnerMu=DatosAdiposeTissue(:,1);
% EnerMu=Ba133ProEnExpHA(:,2)/1000.0; % las energias (MeV) de los puntos
experimentales HA
%
ValorMu=DatosWater(:,2)*rhoWater; % Lineal Attenuation Coefficient (cm-1)
% ValorMu=DatosPb(:,2)*rhoPb; % Lineal Attenuation Coefficient (cm-1)
% ValorMu=DatosAdiposeTissue(:,2)*rhoAT; % Lineal Attenuation Coefficient (cm-1)
% ValorMu=Ba133ProEnExpHA(:,3)*rhoWater; % Valores medidos HA cm-1
[nMu, n0]=size(EnerMu);
%
[nCoef, n3]=size(E_D1);
GammaT=0.0;
xt=(0.001:0.01:100); % rango de espesores cm del material
GammaAtenuado=0.0*xt;
for i=1:nEner; %para cada una de las energias emitidas por el isótopo
correspondiente
    EE=Ener(i)/1000.0; % Energia hay que pasar a MeV
    xx=log(EE);
    for j=1:nCoef;
        if ((EE >= E_D1(j)) && (EE < E_D2(j))) ;
            jE=j;
            Publica_j_Dosis=jE
            break;
        end;
    end;
    DoseEE(i)=exp(C_A(jE)+C_B(jE)*xx+C_C(jE)*xx^2+C_F(jE)*xx^3);
    GammaEE(i)=(Prob(i)*DoseEE(i)); % no hace falta dividir por (4.0*pi*100*100)
    GammaT=GammaT+GammaEE(i);
    for k=1:nMu-1; %valores de la tabla del nist
        %valores de la atenuacion lineal se obtienen por interpolacion a
        %las energias del isotopo
        if((EE >= EnerMu(k)) && (EE <= EnerMu(k+1)) );
            LinearAttenuationEE(i)=ValorMu(k)+(EE-EnerMu(k))*(ValorMu(k+1)-
ValorMu(k))/(EnerMu(k+1)-EnerMu(k)); %unidades cm-1
            break;
        end;
    end;
    GammaAtenuado=GammaAtenuado+GammaEE(i)*exp(-LinearAttenuationEE(i).*xt);
end;
% espesor de corte
corte=GammaT*0.05.*(xt./xt);
corteCero=(GammaAtenuado-GammaT*0.05.*(xt./xt));
[n1, nCorte]=size(xt);
xxtt=1.0;
for m=1:nCorte;
    if((corteCero(m) >= 0.0) && (corteCero(m+1) < 0.0));
        xxtt=xt(m) - corteCero(m)*((xt(m)-xt(m+1))/(corteCero(m)-
corteCero(m+1)));
        PublicaCorte=xxtt
        break;
    end;
end;
%
%
MuAverageWaterCo=0.0632; % en cm-1 atenuacion promedio 60_Co en H2O
MuAveragePbCo=0.670; % en cm-1 atenuacion promedio 60_Co en Pb
MuAverageATXe=0.0601; % en cm-1 atenuacion promedio 60_Co en AT

```

```

%
EaverageBa=153.6387; % en keV
MuAveragePbBa=4.188; % en cm^-1 atenuacion promedio 133_Ba en Pb
MuAverageWaterBa=0.1422; % en cm^-1 atenuacion promedio 133_Ba en H2O
MuAverageATBa=0.1344; % en cm^-1 atenuacion promedio 133_Ba en AT
MuAverageHABa=0.1734; % en cm^-1 atenuacion promedio 133_Ba en HA
%
MuAverageWaterXe=0.2703; % en cm^-1 atenuacion promedio 133_Xe en H2O
MuAveragePbXe=46.6737; % en cm^-1 atenuacion promedio 133_Xe en Pb
MuAverageATXe=0.2323; % en cm^-1 atenuacion promedio 133_Xe en AT
%
MuAverageWaterCs=0.0870; % en cm^-1 atenuacion promedio 137_Cs en H2O
MuAveragePbCs=1.3017; % en cm^-1 atenuacion promedio 137_Cs en Pb
MuAverageATCs=0.0827; % en cm^-1 atenuacion promedio 137_Cs en AT
%
EaverageIr=373.0412; % en keV
MuAveragePbIr=2.334; % en cm^-1 atenuacion promedio 192_Ir en Pb ->
¿?!!!!
MuAverageWaterIr=0.1075; % en cm^-1 atenuacion promedio 192_Ir en H2O
MuAverageATIr=0.1017; % en cm^-1 atenuacion promedio 192_Ir en AT
MuAverageHAIr=0.128; % en cm^-1 atenuacion promedio Extrapolado
graficamente 192_Ir en HA
%
MuAverage=log(20)/xxtt; % en cm^-1 atenuacion promedio
PublicaMuAverage_cm_1=MuAverage
%

%ESTO HAY QUE CAMBIARLO TAMBIEN!!!
PublicaLinearAtt=LinearAttenuationEE./rhoWater % pasar a cm2/g
***densidad***
% PublicaLinearAtt=LinearAttenuationEE./rhoTS % pasar a cm2/g ***densidad***
% PublicaLinearAtt=LinearAttenuationEE./rhoPb % pasar a cm2/g ***densidad***
% PublicaLinearAtt=LinearAttenuationEE./rhoAT % pasar a cm2/g ***densidad***

%
hold off;
% en agua....
plot(Ener,LinearAttenuationEE,'r+');
hold on;
%plot(Ener(nEner),MuAverage,'ro');
plot(EaverageBa,MuAverage,'ro','MarkerFaceColor','r');
hold on;
%
plot(EnerIr,Mu00Ir,'b^');
hold on;
%plot(EnerIr(nEnerIr),MuAverageIr,'bo');
plot(EaverageIr,MuAveragePbIr,'bo','MarkerFaceColor','b');
hold on;
% en AT...
plot(Ener,Mu00AT,'r+');
hold on;
%plot(Ener(nEner),MuAverageATBa,'ro');
plot(EaverageBa,MuAverageATBa,'ro','MarkerFaceColor','r');
hold on;
%
plot(EnerIr,Mu00ATIr,'b^');
hold on;
%plot(EnerIr(nEnerIr),MuAverageATIr,'bo');
plot(EaverageIr,MuAverageATIr,'bo','MarkerFaceColor','b');
hold on;
plot(EnerHABa,Mu00HABa,'r^','MarkerFaceColor','r');
hold on;
%plot(EnerHABa(nEnerHABa),MuAverageHABa,'ro');

```

```

plot(EaverageBa,MuAverageHABa,'ro','MarkerFaceColor','r');
hold on;
plot(EaverageIr,MuAverageHAir,'bo','MarkerFaceColor','b');
hold on;
% error bars
xval=[1 2 3 4 5 6 7 8 9 10];
yval=xval;
for k=1:nEnerHABa;
    deltaval=2*SigmaMu00HABa(k)/9.0;
    for j=1:10;
        xval(j)=EnerHABa(k);
        yval(j)=(Mu00HABa(k)-SigmaMu00HABa(k))+(j-1)*deltaval;
    end;
    plot(xval,yval,'r-');
    hold on;
end;
%

xlabel('Energy / keV'); ylabel('Linear Attenuation Coeff. / cm^-1');
pause;
hold off;
% ahora el espectro de energías con sus probabilidades
plot(Ener,Prob*100.0,'rs');
hold on;
EaverageBa=sum(Ener.*Prob)/sum(Prob);
EnergiaPromedio133Ba=EaverageBa
EaverageIr=sum(EnerIr.*ProbIr)/sum(ProbIr);
EnergiaPromedio192Ir=EaverageIr
%
plot(EnerIr,ProbIr*100.0,'b^');
xlabel('Energy / keV'); ylabel('Probability/(%)');
pause;
hold off;
% dibujar el punto de corte
PublicaGammaOver20=GammaT*0.05
plot(xt,GammaAtenuado,'b+');
hold on;
plot(xt, corte,'r. ');
hold on;
plot(xxTT, GammaT*0.05, 'k^');
xlabel('thickness/cm'); ylabel('Gamma ');
hold off;
pause;

```

- **¹⁹²Ir simulation**

```

%
%
% Dosimetria MOSFET
%
% Rosalía Feal Calvo
% Versión: 14/02/2016
% Dosimetria en MOSFETS localizados en zonas uretral y rectal
%
% agujas paralelas eje OZ
%
%
CTasaIr_00=0.1236; % Constante de la tasa Gy*cm^2/s . Fecha calibrado:
10/09/2013
Thalf=73.827; % Periodo del Ir192 en días
tactual=159; % dias transcurridos a la fecha 21/02/2014
CTasaIr_tactual=CTasaIr_00*exp(-0.69315*tactual/Thalf); % Constante de tasa en
el momento actual
AIr_00=10.897*3.7*1.0E10; % Actividad en el inicio en Bq
AIr_tactual=AIr_00*exp(-0.69315*tactual/Thalf); % Actividad actual en Bq
Gamma_Ir=3.066*1.0E-13; % Constante Gamma del Ir en (Gy*cm^2)/(s*Bq)
%CTasaIr_tactual/AIr_tactual

%%%%%%
%valores de la mu calculados (programa del coeficiente de atenuación másico)

MuAverageIr=0.1069; %en cm^-1 atenuacion promedio 192_Ir en H2O
EaverageIR=400; %energia promedio en keV
MuAverageATIr=0.1017; %en cm^-1 atenuacion promedio 192_Ir en tejido adiposo
%comprobar si la prostata es adiposo o que
MuAverageHAIr=0.128; %en cm^-1 atenuacion promedio 192_Ir en ácido hialurónico

DeltaHAR=1.5; %espesor de capa HA en el recto en cm

% Modelo 1: Todas las agujas se recorren exactamente igual

R_M=0.08; % radio equivalente del MOSFET 0.13 x 0.15 cm^2
Delta_M = 0.30; % tamaño MOSFET 0.30 cm
Vol_M = pi*Delta_M*R_M^2; % Volumen MOSFET para normalizar
%
Zmos_base=[0.7 2.7 4.7 6.7 8.7]; % Posiciones de los MOSFET en cm. Contadas
desde la base. Dimension Nmos
%
Zmos=-1.0.*(Zmos_base-5.0); % La prostata tiene un diametro aproximado de 5 cm
% Por lo tanto ¿hay MOSFET fuera de la prostata? Sí, los hay
% Diametro de la prostata 5 cm y longitud de las agujas 30 cm
% Entonces los puntos de parada habrá que revisarlos ¿no?
%
%
% colocar los MOSFET en un cilindro de radio variable cuyo eje sea una curva
alabeada
%
% en este caso es mejor dar las coordenadas (xagu,yagu) de las agujas que
% supondremos verticales

%
Na=16; % Numero de agujas k=1,...,16
Nmos=5; % numero de MOSFET i=1,...,5
La=30; % Longitud aguja en cm % Atencion!!! 20 o 30?? %Ecografía

```

```
Nstop=16; % Numero de paradas en el recorrido de cada aguja. n=1,2,... , Nstop
%
v_aguja=-La/1; % suponemos que se recorre la aguja en 1 segundos. Datos
contrastados
```

```
%Valores de xagu, yagu, zagu,tagu del caso real estudiado
```

```
xagu=[6.277 7.811 5.523 8.198 6.055 7.976 8.616 5.112 5.199 6.127 7.946 9.007
5.420 6.493 7.469 8.313
6.284 7.819 5.528 8.223 6.074 7.968 8.632 5.114 5.199 6.129 7.942 9.013
5.429 6.509 7.462 8.319
6.290 7.827 5.534 8.249 6.092 7.961 8.648 5.117 5.198 6.131 7.938 9.019
5.438 6.525 7.465 8.324
6.297 7.836 5.539 8.274 6.111 7.954 8.665 5.119 5.198 6.133 7.934 9.025
5.447 6.542 7.467 8.330
6.304 7.844 5.544 8.299 6.130 7.946 8.681 5.122 5.197 6.135 7.930 9.031
5.456 6.558 7.470 8.336
6.310 7.853 5.549 8.325 6.148 7.939 8.697 5.124 5.197 6.137 7.926 9.037
5.465 6.574 7.472 8.342
6.323 7.863 5.555 8.349 6.151 7.938 8.704 5.126 5.196 6.139 7.928 9.043
5.473 6.586 7.474 8.345
6.338 7.876 5.560 8.363 6.126 7.949 8.697 5.129 5.196 6.141 7.938 9.049
5.482 6.590 7.477 8.344
6.354 7.890 5.566 8.377 6.101 7.959 8.690 5.131 5.195 6.142 7.949 9.055
5.491 6.594 7.479 8.342
6.369 7.903 5.571 8.391 6.075 7.969 8.682 5.134 5.195 6.144 7.960 9.061
5.500 6.599 7.482 8.341
6.385 7.917 5.577 8.405 6.050 7.980 8.675 5.136 5.194 6.146 7.971 9.067
5.509 6.603 7.484 8.339
6.400 7.931 5.582 8.419 6.025 7.990 8.668 5.139 5.194 6.148 7.982 9.073
5.518 6.607 7.486 8.338
6.416 7.944 5.588 8.433 6.011 8.001 8.757 5.141 5.193 6.150 7.993 9.079
5.527 6.611 7.492 8.344
6.431 7.958 5.594 8.447 6.021 8.011 8.851 5.143 5.193 6.152 8.004 9.085
5.536 6.615 7.503 8.364
6.447 7.971 5.594 8.461 6.030 8.021 8.870 5.143 5.193 6.154 8.014 9.085
5.536 6.619 7.514 8.383
6.447 7.971 5.594 8.461 6.040 8.032 8.870 5.143 5.193 6.056 8.025 9.085
5.536 6.619 7.514 8.383]; %cm
```

```
yagu=[4.122 4.029 4.746 4.303 4.891 5.194 4.979 5.573 6.105 5.871 5.761 5.920
6.647 6.544 6.394 6.600
4.125 4.052 4.747 4.358 4.904 5.200 4.985 5.572 6.102 5.877 5.769 5.924
6.643 6.552 6.406 6.603
4.129 4.076 4.747 4.414 4.918 5.206 4.990 5.570 6.100 5.882 5.777 5.927
6.639 6.560 6.418 6.606
4.132 4.100 4.748 4.469 4.932 5.213 4.996 5.569 6.097 5.887 5.785 5.931
6.635 6.568 6.430 6.610
4.136 4.123 4.749 4.524 4.945 5.219 5.002 5.567 6.095 5.893 5.793 5.935
6.631 6.576 6.442 6.613
4.140 4.147 4.750 4.580 4.959 5.225 5.008 5.566 6.092 5.898 5.801 5.938
6.627 6.584 6.454 6.616
4.138 4.160 4.744 4.630 4.973 5.226 5.012 5.564 6.090 5.903 5.810 5.942
6.623 6.589 6.467 6.617
4.133 4.155 4.734 4.626 4.987 5.217 5.014 5.563 6.087 5.909 5.819 5.946
6.619 6.586 6.479 6.612
4.128 4.149 4.725 4.622 5.002 5.209 5.016 5.561 6.084 5.914 5.828 5.950
6.615 6.584 6.491 6.607
4.124 4.144 4.716 4.617 5.016 5.201 5.017 5.560 6.082 5.919 5.837 5.953
6.611 6.581 6.503 6.602
4.119 4.138 4.707 4.613 5.031 5.192 5.019 5.558 6.079 5.925 5.847 5.957
6.607 6.578 6.515 6.597
4.114 4.133 4.697 4.609 5.045 5.184 5.021 5.557 6.077 5.930 5.856 5.961
6.603 6.576 6.528 6.592
```

```

4.110 4.127 4.688 4.605 5.054 5.176 5.022 5.555 6.074 5.935 5.865 5.964
6.599 6.573 6.535 6.588
4.105 4.122 4.679 4.600 5.053 5.167 5.022 5.554 6.072 5.941 5.875 5.968
6.595 6.571 6.535 6.585
4.100 4.116 4.679 4.596 5.052 5.159 5.023 5.554 6.072 5.946 5.884 5.968
6.595 6.568 6.534 6.581
4.100 4.116 4.679 4.596 5.050 5.151 5.023 5.554 6.072 5.951 5.893 5.968
6.595 6.568 6.534 6.581]; %cm

```

```
%poner las matrices de zagu y ta
```

```

zagu=[ -6.78 -6.04 -6.90 -5.77 -6.05 -6.09 -6.07 -6.10 -6.10 -6.10
-6.09 -6.10 -6.09 -6.07 -6.09 -6.10
-9.28 -8.53 -9.40 -8.19 -8.54 -8.59 -8.57 -8.60 -8.60 -8.60
-8.59 -8.59 -8.59 -8.56 -8.58 -8.60
-11.78 -11.02 -11.90 -10.62 -11.03 -11.09 -11.06 -11.10 -11.10 -11.10
-11.09 -11.09 -11.09 -11.06 -11.08 -11.09
-14.28 -13.51 -14.40 -13.04 -13.52 -13.59 -13.56 -13.60 -13.60 -13.60
-13.59 -13.59 -13.59 -13.55 -13.58 -13.59
-16.78 -15.99 -16.90 -15.47 -16.01 -16.08 -16.05 -16.10 -16.10 -16.09
-16.09 -16.09 -16.08 -16.04 -16.07 -16.09
-19.28 -18.48 -19.40 -17.89 -18.50 -18.58 -18.54 -18.60 -18.60 -18.59
-18.58 -18.59 -18.58 -18.54 -18.57 -18.59
-21.77 -20.97 -21.90 -20.32 -20.99 -21.08 -21.04 -21.10 -21.10 -21.09
-21.08 -21.09 -21.08 -21.03 -21.07 -21.09
-24.27 -23.47 -24.40 -22.82 -23.47 -23.58 -23.54 -23.60 -23.60 -23.59
-23.58 -23.59 -23.58 -23.53 -23.56 -23.59
-26.76 -25.96 -26.89 -25.31 -25.95 -26.07 -26.04 -26.10 -26.10 -26.09
-26.07 -26.09 -26.08 -26.03 -26.06 -26.09
-29.26 -28.46 -29.39 -27.81 -28.44 -28.57 -28.54 -28.60 -28.60 -28.59
-28.57 -28.59 -28.57 -28.53 -28.56 -28.59
-31.75 -30.95 -31.89 -30.30 -30.92 -31.07 -31.04 -31.10 -31.10 -31.09
-31.07 -31.09 -31.07 -31.03 -31.06 -31.09
-34.25 -33.45 -34.39 -32.80 -33.40 -33.56 -33.53 -33.60 -33.60 -33.59
-33.56 -33.58 -33.57 -33.53 -33.55 -33.59
-36.74 -35.95 -36.88 -35.30 -35.89 -36.06 -35.10 -36.10 -36.10 -36.09
-36.06 -36.08 -36.07 -36.03 -36.05 -36.09
-39.24 -38.44 -39.38 -37.79 -38.39 -38.55 -36.79 -38.60 -38.60 -38.59
-38.55 -38.58 -38.57 -38.53 -38.55 -38.58
-41.73 -40.94 -39.38 -40.29 -40.89 -41.05 -39.28 -38.60 -38.60 -41.09
-41.05 -38.58 -38.57 -41.03 -41.04 -41.07
-41.73 -40.94 -39.38 -40.29 -43.38 -43.55 -39.28 -38.60 -38.60 -43.59
-43.55 -38.58 -38.57 -41.03 -41.04 -41.07]; %mm

```

```
%paso de mm a cm
```

```
zagu=zagu/10;
```

```

tagu=[ 9.57 10.82 6.05 2.85 12.42 16.83 4.19 5.96 5.17 21.17 8.92 5.91
2.75 6.87 9.89 8.10
6.46 6.45 3.18 1.46 6.13 10.83 2.31 3.62 3.43 13.47 3.52 3.92
2.69 4.09 5.42 5.72
4.09 2.75 1.95 1.18 1.26 3.63 1.91 2.21 1.89 5.49 0.06 2.44
2.11 1.82 2.29 4.14
3.13 0.62 1.72 1.91 0.02 0.14 2.22 1.72 1.23 0.65 0.00 2.65
1.86 1.97 1.57 3.65
2.25 1.03 1.23 2.44 0.13 0.01 2.54 2.34 1.22 0.00 0.00 3.22
3.01 3.41 2.82 3.99
3.15 2.93 1.33 2.11 1.13 0.50 3.16 2.35 1.48 0.04 0.04 3.16
3.52 4.81 4.02 4.23
3.51 5.32 1.60 1.26 2.30 1.68 2.79 2.07 1.77 0.31 0.45 3.38
3.30 5.70 4.47 2.76
2.46 5.43 1.39 1.06 3.15 2.38 2.37 2.56 1.46 0.66 1.34 2.03
2.48 5.16 4.02 1.04

```

```

1.77 2.29 4.21 2.04 0.76 3.79 2.42 2.50 2.74 1.42 0.86 1.93 0.85
4.08 2.95 1.57
2.13 3.45 2.34 1.71 0.97 4.09 2.03 2.05 1.84 1.29 1.54 1.73 1.69
2.91 1.53 2.42
1.95 2.61 2.35 1.12 1.13 3.93 2.02 0.65 1.15 1.09 1.80 1.85 1.79
2.47 1.47 2.26
2.05 3.49 2.93 1.19 1.09 4.25 2.94 0.00 1.16 1.71 2.13 2.24 2.10
2.60 1.72 2.49
2.98 6.42 4.56 1.66 1.22 3.55 3.53 0.55 1.54 3.31 3.03 1.57 3.40
1.97 2.29 3.49
4.07 10.27 6.00 2.28 1.89 2.57 4.33 1.87 2.32 4.37 4.73 1.17 4.67
1.40 3.44 4.51
0.00 12.02 6.66 0.00 2.88 2.03 5.30 3.30 0.00 0.00 8.95 2.61 0.00
2.81 4.69 5.48
0.00 0.00 0.00 0.00 1.83 7.60 0.00 0.00 0.00 11.78 3.95 0.00
0.00 0.00 0.00 0.00]; %s

```

```

%atención porque el centro de las agujas puede que no coincide con el
%centro de la próstata en ocasiones especiales
xcentroagu=sum(xagu(1,:))/Na;
ycentroagu=sum(yagu(1,:))/Na;
xagu=xagu-xcentroagu;
yagu=yagu-ycentroagu;
%
% ahora la curva paramétrica y la helicoides
% la curva es el eje de la uretra. La helicoides recorre la superficie
% cilíndrica de la uretra
%
radio=0.30;
radio_recto=0.75;
alfa=0.50;
alfa_recto=-2.65-DeltaHAR; % valor x inicial de la zona rectal -> suponemos que
la próstata está en la región de las z negativas
%y suponemos que tiene un diámetro de 5 cm
beta=100;
zeta_uretra=-5.5; %cm
zeta_recto=-5.5; % zeta punto inicial de la zona rectal en cm
s0=0:0.0001/pi:0.270/pi; % Mucha atención a las dimensiones (longitud y
diámetro) del tubo de la uretra, por ejemplo.
s=pi.*s0;
nturns=50; % numero de vueltas helicoidales al eje del tubo
t=(nturns*2*pi/(0.270/pi)).*s0;
% El eje una parábola en el plano OXZ x=alfa-s, y=0, z=beta*s^2
% Longitud del eje de la uretra. Debería ser 6 cm
ntubo=length(s);
smax=max(s);
Long_eje=0.50*smax*sqrt(1.0+4.0*beta^2*smax^2)+(0.25/beta)*log(2.0*beta*smax+sqrt
(1+4.0*beta^2*smax^2));
Longitud=Long_eje
%
% en primera opción Radio Constante R=0.5 cm R(s)
% RMOS_XYZ=[-s+radio.*cos(t)*2.0*beta.*s./sqrt(1.0+4.0*beta^2*s.^2)
radio.*sin(t) beta*s.^2+radio.*cos(t)/sqrt(1.0+beta^2*4.0*s.^2)];
% RMOS_XYZ son las "posibles" posiciones de los mosfet en la superficie de
% la uretra y de la zona del recto....
%
XMOS=alfa-s+radio.*cos(t)*beta*2.0.*s./sqrt(1.0+(beta^2*4.0).*s.^2);
YMOS=radio.*sin(t);
ZMOS=zeta_uretra+beta.*s.^2+radio.*cos(t)./sqrt(1.0+(beta^2*4.0).*s.^2);
%
XMOS_recto=alfa_recto-s+radio_recto.*cos(t)*beta*2.0.*s./sqrt(1.0+
(beta^2*4.0).*s.^2);
YMOS_recto=radio_recto.*sin(t);

```

```

ZMOS_recto=zeta_recto+beta.*s.^2+radio_recto.*cos(t)./sqrt(1.0+
(beta^2*4.0).*s.^2);
%
%
XMOSeje=alfa-s;
YMOSeje=0.0.*s;
ZMOSeje=beta.*s.^2;
%
figure(1);
xlabel('X (cm)');
ylabel('Y (cm)');
zlabel('Z (cm)');
axis([-4 4 -4.0 4.0 -5 1])
hold on;
grid on;
pause;
%
plot3(XMOSeje, YMOSeje, ZMOSeje+zeta_uretra, 'r-');           % eje del tubo
uretral
pause;
hold on;
plot3(XMOS, YMOS, ZMOS);   % helicoide recorriendo la pared del tubo uretral
hold on;
pause;
hold on;
plot3((XMOSeje-alfa+alfa_recto), YMOSeje, ZMOSeje+zeta_recto, 'r-'); % eje del
tubo rectal
pause;
hold on;
%
plot3(XMOS_recto, YMOS_recto, ZMOS_recto, 'g-'); % helicoide recorriendo la
pared del tubo rectal
pause;
hold on;

npuntos=19;
[xp, yp, zp] = ellipsoid(0,0,-2.5,2.45,1.81,2.22,npuntos); % aqui simulamos la
prostata con un elipsoide atencion a las dimensiones
% prueba de las coordenas del elipsoide ¿hay que entender estas
coordenadas????
xprostata=xp;
yprostata=yp;
zprostata=zp;

zmaximo=max(zprostata);

%se refieren las coordenadas de forma que este punto máximo de la próstata
%sea Z0
%
surfl(xp, yp, zp)
colormap copper
%axis equal
hold on;
% para dibujar las posiciones de las agujas
% habría que construir una matriz con las coordenadas (Xagu,Yagu) de todas las
agujas
radio=0.030;
[xc,yc,zc] = cylinder(radio,npuntos);
%
xcilindro=xc;
ycilindro=yc;
zcilindro=zc;
% dibujar las agujas
for k=1:Na;

```

```

surf(xc+xagu(1,k), yc+yagu(1,k), 1.*zc);
hold on;
surf(xc+xagu(1,k), yc+yagu(1,k), -6.*zc);
end;
pause;
hold off;

%%%%%%%%%%%%%%%%%%%%%%%%%%%%%%%%%%%%%%%%%%%%%%%%%%%%%%%%%%%%%%%%%%%%%%%%
% % % % % % % % % % % % % % % % % % % % % % % % % % % % % % % % % % %
%
%           ahora la dosis a lo largo de las paredes del tubo uretral
%           se calculan las dosis en los puntos de la helicoides
%
DosisMOSTubo=0.0.*s;           % inicializar valor de dosis en cada punto de
la pared del tubo
DosisMOS_IntegradaTubo=0.0.*s; % inicializar valor de dosis en cada MOSFET
Integrado al volumen MOSFET
DosisEncadaMOSTubo=DosisMOSTubo; % debida al recorrido de la aguja a velocidad
constante de una posicion a otra
%
%
ZmosTubo=ZMOS;
rhoMOSTubo=eye(Na,ntubo);

for i=1:ntubo; % i=indice del punto del tubo donde van los MOSFET
for k=1:Na; % k=indice de la aguja %significa fijar x, y aguja
% calcular la distncia rho entre aguja k y el punto i del tubo de
% los MOSFET

Xa=xagu(:,k);
Ya=yagu(:,k);
Za=zagu(:,k);
Ta=tagu(:,k);

for n=1:Nstop; % n=indice de la parada en cada aguja

rhoMOSTubo(k,i)=sqrt((Xa(n)-XMOS(i))^2+(Ya(n)-YMOS(i))^2);
disfuentemOSTubo=sqrt((rhoMOSTubo(k,i))^2+(Za(n)-ZmosTubo(i))^2);
disfuentemOSTubo0=sqrt(rhoMOSTubo(k,i)^2+(Za(n)-ZmosTubo(i))^2);
DeltaTubo=disfuentemOSTubo-disfuentemOSTubo0;
DosisMOSTubo(i)=DosisMOSTubo(i)+
(CTasaIr_tactual*Ta(n)/disfuentemOSTubo^2)*exp(-
disfuentemOSTubo0*MuAverageATIr)*exp(-DeltaTubo*MuAverageHAIr);

end;

% suponemos que la extraccion de la aguja aporta lo mismo que en
% el recorrido de entrada: factor 2.0*
DosisEncadaMOSTubo(i)=DosisEncadaMOSTubo(i)+2.0*(CTasaIr_tactual/
(rhoMOSTubo(k,i)*v_aguja))*(atan(-La-ZmosTubo(i))+atan(ZmosTubo(i)));
%
U_M=(R_M/rhoMOSTubo(k,i))^2;
UMenos=(1.0-U_M);
IR1=Vol_M*(1.0+((1.0/3.0+pi/2.0)/pi)*U_M)/rhoMOSTubo(k,i)^2;
%

%atención a los valores de Z(a) y de los tiempos Ta para esta aguja -> 16x16

end;
end;

```

```

%
zeta= ZmosTubo; % Posicion del MOSFET
DosisParadasMOS=DosisMOSTubo; % Contribución de las paradas
DosisMOS_IntegradaTubo=DosisMOS_IntegradaTubo./Vol_M; % aproximacion promedio
al volumen del MOSFET. Las Paradas
DosisRecorridoMOS=DosisEncadaMOSTubo; % contribucion del recorrido de la
aguja
% parece que el error asociado a las fluctuaciones poissonianas de la
% actividad va a ser irrelevante porque las muestras son muy muy activas ¿?
%
figure(2);
plot(ZmosTubo,DosisMOSTubo,'r^'); %contribucion de las paradas
hold on;
pause;
plot(ZmosTubo,DosisEncadaMOSTubo,'go'); % contribucion de los viajes de ida y
vuelta de las agujas
hold on;
% plot(ZmosTubo,DosisMOSTubo+DosisEncadaMOSTubo,'r+'); % contribucion total
% hold on;
%plot(ZmosTubo,DosisMOS_IntegradaTubo,'b*'); % contribucion total calculada
integrando
pause;
xlabel('Uretral MOSFET location (cm)');
ylabel('Total Dosis (Gy)');
axis([-7 3 0 9]);
%
pause;
hold off;
%
% % % % % % % % % % % % % % % % % % % % % % % % % % % % % % % % % % %
%
% dosis a lo largo de las paredes del tubo zona rectal
% se calculan las dosis en los puntos de la helicoide
%
DosisMOSTuboR=0.0.*s; % inicializar valor de dosis en cada punto de
la pared del tubo
DosisMOS_IntegradaTuboR=0.0.*s; % inicializar valor de dosis en cada MOSFET
Integrado al volumen MOSFET
DosisEncadaMOSTuboR=DosisMOSTuboR; % debida al recorrido de la aguja a velocidad
constante de una posicion a otra
%

ZmosTuboR=ZMOS_recto;
rhoMOSTuboR=eye(Na,ntubo);
for i=1:ntubo; % i=indice del punto del tubo rectal donde van los MOSFET
    for k=1:Na; % k=indice de la aguja
        Xa=xagu(:,k);
        Ya=yagu(:,k);
        Za=zagu(:,k);
        Ta=tagu(:,k);

        for n=1:Nstop; % n=indice de la parada en cada aguja

            % calcular la distancia rho entre aguja k y posición n y el punto i
del tubo donde van los MOSFET
            rhoMOSTuboR(k,i)=sqrt((Xa(n)-XMOS_recto(i))^2+(Ya(n)-
YMOS_recto(i))^2);
            disfuenteMOSTuboR=sqrt((rhoMOSTuboR(k,i)+DeltaHAR)^2+(Za(n)-
ZmosTuboR(i))^2);
            disfuenteMOSTuboR0=sqrt(rhoMOSTuboR(k,i)^2+(Za(n)-ZmosTuboR(i))^2);
            DeltaRTuboR=disfuenteMOSTuboR-disfuenteMOSTuboR0;
            DosisMOSTuboR(i)=DosisMOSTuboR(i)+
( CTasaIr_tactual*Ta(n)/disfuenteMOSTuboR^2)*exp(-
disfuenteMOSTuboR0*MuAverageATIr)*exp(-DeltaRTuboR*MuAverageHAIr);

```

```

        % por integracon con promedio en angulo theta

    end;

    %suponemos que la extraccion de la aguja aporta lo mismo que en el
    recorrido de entrada: factor 2.0*
    DosisEncadaMOSTuboR(i)=DosisEncadaMOSTuboR(i)+2.0*(CTasaIr_tactual/
    (rhoMOSTuboR(k,i)*v_aguja))*(atan(-La-ZmosTuboR(i))+atan(ZmosTuboR(i)));
    %
    U_M=(R_M/rhoMOSTuboR(k,i))^2;
    UMenos=(1.0-U_M);
    IR1=Vol_M*(1.0+((1.0/3.0+pi/2.0)/pi)*U_M)/rhoMOSTuboR(k,i)^2;
end;
end;

%
zetaR= ZmosTuboR;          % Posicion del MOSFET
DosisParadasMOSRecto=DosisMOSTuboR;          % Contribución de las paradas
DosisMOS_IntegradaTuboR=DosisMOS_IntegradaTuboR./Vol_M; % aproximacion promedio
al volumen del MOSFET. Las Paradas
DosisRecorridoMOSRecto=DosisEncadaMOSTuboR;   % contribucion del recorrido de
la aguja
% parece que el error asociado a las fluctuaciones poissonianas de la actividad
va a ser irrelevante porque las muestras son muy muy activas ;?
%

%
figure(3);
plot(ZmosTuboR,DosisMOSTuboR,'r^'); %contribucion de las paradas en las agujas
hold on;
pause;
plot(ZmosTuboR,DosisEncadaMOSTuboR,'go'); % contribucion de los viajes de ida y
vuelta de las agujas
hold on;
pause;
% plot(ZmosTubo,DosisMOSTubo+DosisEncadaMOSTubo,'r+'); % contribucion total
% hold on;
% plot(ZmosTuboR,DosisMOS_IntegradaTuboR,'b*'); % contribucion de las paradas
calculada integrando
% hold on;
% pause;
xlabel('Rectal MOSFET location (cm)');
ylabel('Total Dosis (Gy)');
axis([-8 4 0 7.3]);
%
%
pause;
hold off;
%

```

- **¹³³Xe simulation**
- **¹³³Ba simulation**
- **¹³⁷Cs simulation**
- **⁶⁰Co simulation**

The MatLab program is the same one used for ¹⁹²Ir simulation, but changing the values of *MuAverage*, *Eaverage*, *MuAverageAT* and *MuAverageHA*; and supposing that all activities are the same through $C_{Tasa\ actual}(Xe) = \Gamma(Xe) \cdot A_0(Ir)$